Advances in Continuous and Discrete Models

REVIEW Open Access

Bond-based peridynamics, a survey prospecting nonlocal theories of fluid-dynamics

Nunzio Dimola[1], Alessandro Coclite[1*], Giuseppe Fanizza[2] and Tiziano Politi[1]

*Correspondence:
alessandro.coclite@poliba.it
[1]Dipartimento di Ingegneria Elettrica e dell'Informazione, Politecnico di Bari, Via Re David 200, 70125 Bari, Italy
Full list of author information is available at the end of the article

Abstract

Peridynamic (PD) theories have become widespread in various research areas due to the ability of modeling discontinuity formation and evolution in materials. Bond-based peridynamics (BB-PD), notwithstanding some modeling limitations, is widely employed in numerical simulations due to its easy implementation combined with physical intuitiveness and stability. In this paper, we review and investigate several aspects of bond-based peridynamic models. We present a detailed description of peridynamics theory, applications, and numerical models. We display the employed BB-PD integral kernels together with their differences and commonalities; then we discuss some consequences of their mathematical structure. We critically analyze and comment on the kinematic role of nonlocality, the relation between kernel structure and material impenetrability, and the role of PD kernel nonlinearity in crack formation prediction. Finally, we propose and present the idea of extending BB-PD to fluids in the framework of fading memory material, drawing some perspectives for a deeper and more comprehensive understanding of the peridynamics in fluids.

MSC: 74A70; 74B20; 70G70; 35Q70; 74S20

Keywords: Peridynamics; Nonlocal continuum mechanics; Numerical methods; Nonlocal fluids

1 Introduction

Peridynamics (PD) is a nonlocal continuum mechanics theory introduced by Silling [1] to mathematically describe fracture formation and development in elastic materials. To overcome limitations imposed by the classical theory, which results inadequate in treatment of spatial discontinuities eventually occurring in material bodies, in the peridynamic equation of motion, an integral operator takes the place of spatial derivatives. The process of integration holds its consistency even with very irregular functions, so that discontinuous displacements (i.e., cracks) are still significant in the peridynamics framework. The growing interest of the scientific community in peridynamics [2] is motivated by the fact that such a theory could constitute a linking connection between atomistic theories of matter and classical continuum mechanics. Consequently, microscale phenomena, like wave

dispersion [3–6], cracks [7–11], intragranular fracture [12], etc., could be modeled even in macroscopic structures by a suitable tuning of the *peridynamic horizon* length, which rules the extent of nonlocal interactions between a point of the body and the surrounding ones [13]. Firstly, the so-called *bond-based* (BB) peridynamic has been introduced in [1], where the internal forces between a point and all the other ones inside its peridynamic horizon are modeled as a central force field. We can figure such a force field as a network of bonds linking each point of the body with every point within its horizon. Then, to overcome bond-based PD modeling limitations for Poisson's ratio [14–17] (1/3 for the plane stress and 1/4 for the plane strain in 2D bodies, and 1/4 for 3D ones), a generalized peridynamics theory, *state-base* peridynamics, has been formulated in [18]. In this context the force exchanged between a point and another one in its horizon does not depend solely on their bond extension, but also on the deformation state of all other bonds relative to the horizon. Note that peridynamics theories differ from classical mechanics for the presence of such finite-range bonds between any two points of the material body, which is a feature that assimilates such formulations to discrete mesoscale theories of matter. In the PD framework, physical bodies are considered as formed by a continuous network of points exchanging momentum within a fixed interaction distance $\delta > 0$, the horizon radius; this change of paradigm, much closer to molecular dynamics than macroscopic bodies one, allows us to abandon the local concept of stress tensor and move on to the concept of *pairwise force* (see Fig. 1a,c). In a Lagrangian framework, best suited for finite deformations, the peridynamic horizon is fixed in the reference configuration and deforms with the body [14]. Conversely, when viscoelastic materials or fluids (which are naturally

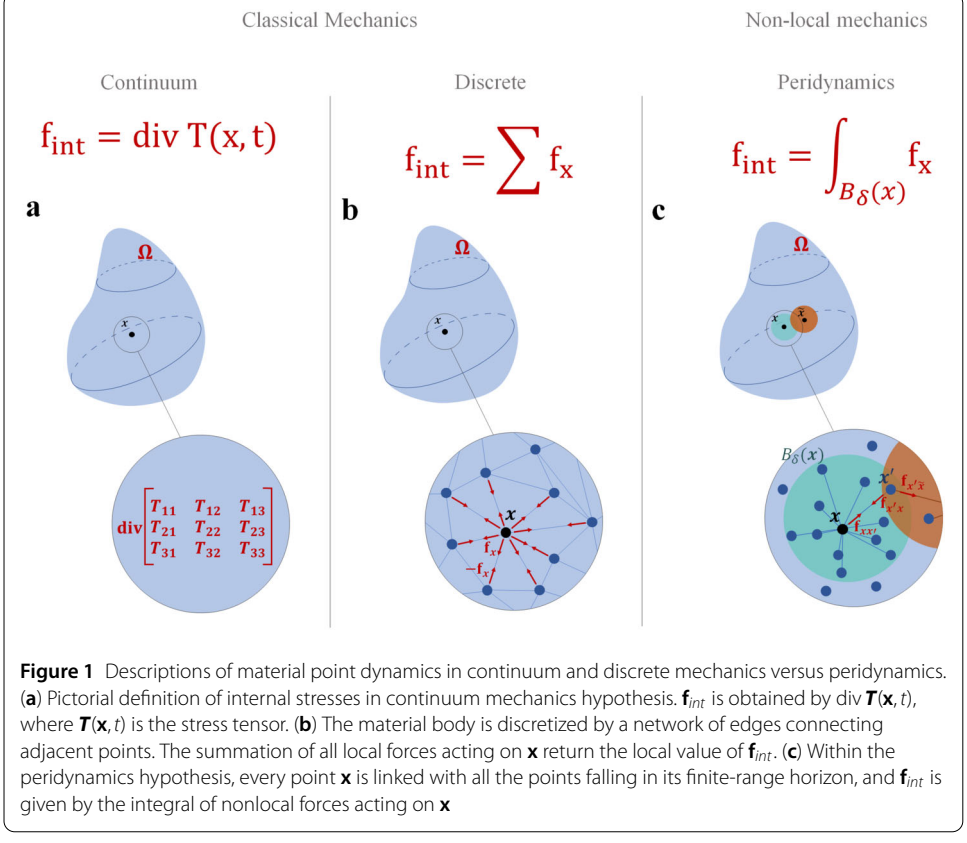

Figure 1 Descriptions of material point dynamics in continuum and discrete mechanics versus peridynamics. (**a**) Pictorial definition of internal stresses in continuum mechanics hypothesis. $\mathbf{f}_{int}$ is obtained by div $\boldsymbol{T}(\mathbf{x}, t)$, where $\boldsymbol{T}(\mathbf{x}, t)$ is the stress tensor. (**b**) The material body is discretized by a network of edges connecting adjacent points. The summation of all local forces acting on $\mathbf{x}$ return the local value of $\mathbf{f}_{int}$. (**c**) Within the peridynamics hypothesis, every point $\mathbf{x}$ is linked with all the points falling in its finite-range horizon, and $\mathbf{f}_{int}$ is given by the integral of nonlocal forces acting on $\mathbf{x}$

subjected to very large deformations) are considered, it is more physically reasonable to maintain the PD horizon fixed in time, so that its shape never changes as the body deforms. This approach is known in the literature as Eulerian [19] or semi-Lagrangian [20] peridynamics.

Due to its flexibility, beyond already mentioned research fields (crack formation and propagation in elastic material, wave dispersion in material, intragranular fracture), the peridynamics nonlocal approach to discontinuities has found applications in several research areas. In geomechanics, PD has been employed in water-induced soil cracks [21, 22], geomaterial failure [23], rocks fragmentation [24], etc. (see [25]). In biology, long-range interactions in living tissues [26], cellular ruptures, cracking of biomembranes [27], and so on [2] have been analyzed within peridynamics framework. In [28–30] a peridynamic theory for thermal diffusion has been introduced to model heat conduction in materials featuring spatial discontinuities, defects, inhomogeneities, and cracks. Advection–diffusion behavior in PD has been studied in [31] for modeling fingering phenomenon for multiphase fluids in porous media, and in [32] a constructive PD model for transient advection–diffusion problems has been presented. Being a plethora of physical phenomena modeled consistently by peridynamics, various multiphysics analysis have been performed within PD scheme, e.g., microstructural analysis [33], fatigue [34] and heat conduction [35] in composite materials, galvanic corrosion in metals [36], electricity-induced cracks in dielectric materials [37], and so forth.

Significant similarities between bond-based peridynamics theory and discrete theory of materials can be pointed out. Indeed, in discrete theories of matter, a material body is thought as formed by a discrete network of points linked with spring-like bonds. Each point exerts long-range elastic interaction with all others with which it shares a bond. Thus each point belonging to this discrete network can be associated with a discrete set of finite-range interacting points, equivalent to the PD horizon (see Fig. 1b). Both in PD and discrete theories, linear and angular momentum balance is not guaranteed locally, so a process of summation for discrete network or integration for continuous one over all points that constitute the material body is necessary. Given such similarities between material PD theory and discrete one, it is not surprising that most of the scientific efforts have been directed toward a numerical implementation of the peridynamic equation. Apart from PD theory, discontinuities formation and development in material structures have been more or less satisfactory addressed by enhanced versions of classical continuum mechanics numerical methods (like smoothed particle hydrodynamics (SPH) [38, 39], extended finite element (xFEM) [40], cohesive zone (CZM) methods [41], and so on); however, peridynamics appeal stems from the lack of external criteria and adjoined degrees of freedom to the numerical schemes. Neglecting some exceptions, PD numerical analysis can be grossly divided into two macroarea, PD finite element analysis and mesh-free methods or, equivalently, quadrature methods [2, 42]. Such a division is solely for summarizing purposes, and a plethora of subdivisions, parallelisms, and couplings can be found in the literature. Moreover, further numerical methods, like spectral methods [43–45], considering or neglecting the volume penalization step [46, 47], boundary element methods (BEMs) [48] have been developed recently in the context of peridynamics, enlarging the range of available PD numerical tools. In [49] a mesh-free method has been developed to numerically solve the PD equation for so-called prototype microelastic brittle (PMB) materials, showing that the stability criterion for the proposed numerical scheme weakly depends on space

discretization, but the results are principally dictated by the peridynamic horizon size. In [50], mathematical well-posedness of the elastic one-dimensional PD Cauchy problem has been proved, and a proposed numerical quadrature method for the PD integrodifferential equation (IDE) was shown to converge to analytical solutions both for continuous and discontinuous initial conditions. Convergence in mesh-free peridynamics simulations has been analyzed in [51] for 1D, 2D bond-based PD, and 3D state-based PD, considering static problems; convergence of the numerical scheme, under mesh refinement (δ kept constant), to a manufactured nonlocal analytical solution has been shown. Two methods for mitigating the so-called *partial volume* effect, i.e., the intersection discrepancy between the circular/spherical shape of the PD horizon and the polygonal shape of grid cells have been proposed, one based on more accurate analytic calculations of such intersection contribution and the other based on employing compactly supported smooth micromodulus functions, i.e., functions vanishing at the horizon boundary, so that the intersected volumes contribution is minimized. In [52], close connections between peridynamics and classical mesh-free methods have been established. State-based PD is shown to be a numerically faster case of the so-called reproducing kernel particle methods (RKPMs), so that the same approach employed in RKPM boundaries treating could be extended to state-based PD, developing the *reproducing kernel* peridynamics. Mesh refinement strategy for numerical analysis of 1D peridynamic elastic bodies has been introduced by [53]; convergence of the numerical solution to the classical elastic one has been proven for vanishing PD horizon ($\delta \to 0$) and compared for various employed micromodulus function shapes; the so-called *visibility criterion* was introduced as a refinement approach.

It is a well-known fact that in correspondence to the interface between refined and coarsen mesh regions, spurious phenomena like volume losses, ghost forces, and surface softening may occur [54–56]. In [57] the concept of *dual horizon* has been firstly introduced: the total internal force acting at a point of the body is split between a reaction force component due to the interactions of a point with its neighborhood (because of Newton's third law) and an active force component exerted on the point by its dual horizon. In such a way, peridynamics forces are defined consistently also in correspondence with refined mesh interfaces, where different horizon length coexists. The dual horizon concept has been applied in [58] to discretized bond-based PD, together with Voronoi-based adaptive mesh refinement, showing good agreement with standard peridynamics test cases. In [59] a careful approach is adopted in mesh adaptive refinement by the introduction of fictitious nodes near the interface region between the coarse and refined mesh. As a result, spurious phenomena are considerably reduced. In [60], mesh influence on PD numerical solution has been explored in a bond-based PD framework. The onset of periodic patterns in the integration error for 1D configuration, accuracy loss caused by perturbations of quadrature points location in 2D configuration, and unrealistic crack patterns in 3D impact simulations have been observed and directly linked to grid Cartesian structure and simplistic quadrature strategies, pointing out that accurate discretization schemes must be employed for preventing mesh sensitivity in PD numerical simulations.

Concurrently, finite element methods (FEMs) have been extended to peridynamics theory. In [15], peridynamics extensibility to finite elements method coding has been proved and tested using ABAQUS® FEM code for impact simulations, showing great prediction capabilities. Given the wide spread of commercial FEM codes in engineering, the interest in couplings between FEM code and PD theory has rapidly increased. In [61] a coupling

between FEM and peridynamics has been carried out to take advantage of the peculiarities of both FEM and PD approaches, i.e., fast numerical efficiency and inherent crack prediction capabilities, respectively. The peridynamics approach has been employed only for domain portions where damage was expected to occur, whereas the FEM approach has been employed for no-expected-damage zones. Application of continuous and discontinuous Galerkin finite element methods to PD has been explored in [62] and validated against 1D peridynamics exact solutions. In [63] a fast and cost-efficient Galerkin method developed in [64] has been extended and improved for 1D linearized PD static problems providing *hp*-adaptivity, reducing computational efforts and memory usage. In [65] the implementation of a coupled PD-FEM approach in commercial software ABAQUS® has been performed, employing mesh coupling techniques developed in [66–68], with good results, whereas, recently, in [69] a PD-FEM coupled approach has been carried out with the commercial software ANSYS® for fatigue prediction in materials.

Although bond-based PD is the most dated formulation of peridynamics and suffers of the discussed Poisson ratio limitation, it is yet employed in several numerical studies on peridynamics. Physical intuitiveness, less computational efforts, and crack simulation stability concerning state-based PD make the choice of bond-based integral kernel still attractive [70, 71], so much that several extension of bond-based PD has been proposed (for a review, refer to [71]).

In bond-based numerical analysis, different types of integral kernels have been employed to model different kinds of nonlocal interactions, characteristics of the analyzed material, and/or structure. Various micromodulus functions have been studied and tested in the classical or *linearized* version of BB-PD, resulting in a great variety of constitutive models. At the same time, the fundamental structure of the BB peridynamics kernel, with few exceptions [43, 44, 72], has not varied so much from the prototype microelastic brittle (PMB) material (e.g., [7, 73, 74], among others), which is fundamentally a *linear* model. A clarification must be done: with a linear (nonlinear) model, we design all those PD kernels that are linear (nonlinear) in the displacement variable and undergo a *finite* displacement; by a *linearized* model we mean every BB-PD integral kernel linearized (via Taylor expansion) with respect to the relative displacement variable, i.e., that undergo, for small relative displacements, a first-order approximation of the pairwise force.

The great flexibility in choosing a peridynamics kernel, however, addresses a fundamental question: how do physical principles reflect on the structure of the peridynamic equations? Or, conversely, which physic emerges according to the different kernel structures with which peridynamic theory is presented? This paper aims to shed light on the questions above to highlight common features between widespread linear and nonlinear peridynamics bond-based models for hyperelastic materials and to shape some future perspectives for a wider understanding of kernel structure-related physical and numerical peculiarities.

Basic ideas, concepts, and physical assumptions of peridynamics bond-based theory in Lagrangian formalism are illustrated in Sect. 2. A review of bond-based integral kernels employed in the literature is presented in Sect. 3, underlying their features, structures, and properties. In Sect. 4.1 the kinematics aspects of peridynamics nonlocality property are highlighted, compared with those of classical continuum mechanics, and related to the concept of the finiteness of bond stretch. The influence of PD kernel structure on the basic requirement of impenetrability of the matter is explored in Sect. 4.2. The potential role of

peridynamic kernel nonlinearity as a substitute for the classical critical-stretch criterion in material damage prediction is formulated in Sect. 4.3. Finally, in Sect. 5, some perspectives are traced for the application of bond-based peridynamic to fluids. Fluids and solids are compared in their constitutive behavior' then by making use of the merging concept of fading memory some aspects of an extension of PD formalism toward fluids have been formally highlighted.

2 Peridynamics foundation

Let a subset $\Omega \subset \mathbb{R}^n$ with $n \in \{1, 2, 3\}$ represent a material body with constant density $\rho > 0$. At time $t = 0$, such a material body encloses the volume $\Omega_0 \subset \mathbb{R}^n$ taken as its reference configuration. Note that the reference configuration may correspond either to the stress-free configuration or to a given configuration of the body taken as reference. As discussed, in the peridynamics hypothesis, each point of the material body interacts with all the points $\mathbf{x}'$ falling within a certain neighborhood $B_\delta(\mathbf{x}) = \{\mathbf{x} : d(\mathbf{x}, \mathbf{x}') \leq \delta\}$, where $\delta > 0$, and $d(\cdot, \cdot)$ is a suitable distance on Ω_0 (see Fig. 2b); in the literature, it is usually referenced either as the *horizon* (e.g., in [1, 49, 57]) or the *family* of $\mathbf{x}$ (e.g., in [14, 75, 76]). Here the kinematics of $\mathbf{x}$ is given in terms of its displacement with respect to the reference position, namely $\mathbf{u}(\mathbf{x}, t) : \Omega_0 \times \mathbb{R}^+ \to \mathbb{R}^n$. As a consequence, the position of $\mathbf{x}$ at a certain t is given by $\mathbf{y}(\mathbf{x}, t) := \mathbf{x} + \mathbf{u}(\mathbf{x}, t)$ (see Fig. 2a). Moreover, for each couple of interacting points, the

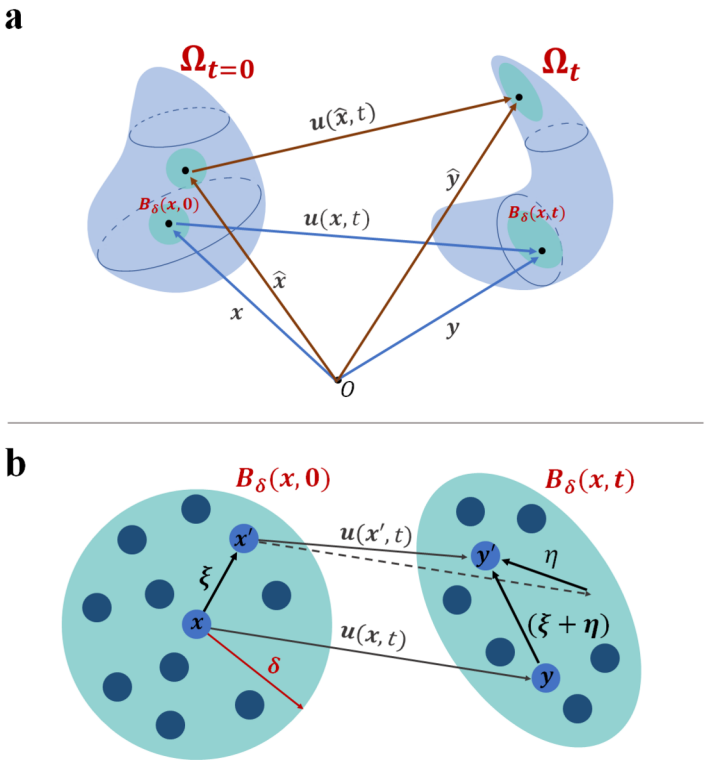

Figure 2 Points kinematic and range of interactions in peridynamics. (**a**) All points in the reference configuration $\Omega_{t=0} \equiv \Omega_0$ are labeled through a ray-vector starting at the origin of Ω_0. The displacement functions $\mathbf{u}(\mathbf{x}, t)$ associate a point into the deformed configuration Ω_t with each point of Ω_0. Indeed, at $t > 0$ a point in Ω_t is completely characterized by $\mathbf{x}(t) = \mathbf{x}(0) + \mathbf{u}(\mathbf{x}, t)$ (**b**) Deformation in time of the ball $B_\delta(\mathbf{x})$ made up by all points $\mathbf{x}'$ such that $|\mathbf{x} - \mathbf{x}'| \leq \delta$

length of the pairwise bond relatively to the initial configuration is tracked in time by the relative strain

$$s\big(\mathbf{x},\mathbf{x}',t\big)=\frac{|\mathbf{u}(\mathbf{x}',t)-\mathbf{u}(\mathbf{x},t)|}{|\mathbf{x}'-\mathbf{x}|}, \tag{2.1}$$

where $|\cdot|$ is the Euclidean norm. Such pairwise bonds length varies in time responding to the force per unit volume squared $\mathbf{f}(\mathbf{x}',\mathbf{x},\mathbf{u}'(\mathbf{x}),\mathbf{u}(\mathbf{x}),t)$. Note that the dependence of $\mathbf{u}$ on t is omitted to simplify the notation. Alongside $\mathbf{f}$, an external forcing term $\mathbf{b}(\mathbf{x},t)$ is provided, so that the Lagrangian balance equation for the momentum of $\mathbf{x}$ reads

$$\rho\mathbf{u}_{tt}(\mathbf{x},t)=\mathbf{F}(\mathbf{x},t), \tag{2.2}$$

where $\mathbf{F}(\mathbf{x},t)$ is the sum of all internal and external per-unit-volume forces acting on $\mathbf{x}$:

$$\mathbf{F}(\mathbf{x},t)=\int_{\Omega_0\cap B_\delta(\mathbf{x})}\mathbf{f}\big(\mathbf{x}',\mathbf{x},\mathbf{u}\big(\mathbf{x}'\big),\mathbf{u}(\mathbf{x})\big)\,dV_{\mathbf{x}'}+\mathbf{b}(\mathbf{x},t). \tag{2.3}$$

Within the hypotheses of *homogeneity* of the material and *invariance with respect to rigid motion*, the pairwise interaction reduces to a function of $\mathbf{x}'-\mathbf{x}$ and $\mathbf{u}(\mathbf{x}')-\mathbf{u}(x)$. This momentum balance equation is enriched by initial conditions, and the Cauchy problem responding to nonlocal interactions reads

$$\begin{cases}\rho\mathbf{u}_{tt}(\mathbf{x},t)=(\mathbf{K}\mathbf{u}(\cdot,t))(\mathbf{x})+\mathbf{b}(\mathbf{x},t), & t>0,\mathbf{x}\in\Omega_0,\\ \mathbf{u}(\mathbf{x},0)=\mathbf{u}_0(\mathbf{x}),\\ \partial_t\mathbf{u}(\mathbf{x},0)=\mathbf{v}_0(\mathbf{x}),\end{cases} \tag{2.4}$$

where

$$(\mathbf{K}\mathbf{u})(\mathbf{x}):=\int_{\Omega_0\cap B_\delta(\mathbf{x})}\mathbf{f}\big(\mathbf{x}'-\mathbf{x},\mathbf{u}\big(\mathbf{x}'\big)-\mathbf{u}(\mathbf{x})\big)\,dV_{\mathbf{x}'},\quad \mathbf{x}\in\Omega_0. \tag{2.5}$$

We consider only closed manifolds, so that no boundary conditions are required. Looking at (2.4), it is worth noting that no spatial derivatives are involved in the evolution equation of $\mathbf{x}$, so the integrodifferential equation still remains valid for regions characterized by discontinuous displacements (crack, phase changing region, etc.): this represents a great advantage of the peridynamic theory of continuum.

If external forces in Eq. (2.4) are neglected, it becomes manifest that only the kernel structure of $(\mathbf{K}\mathbf{u})$ influences the whole problem from both mathematical and physical points of view; that is, the mathematical structure of the evolution problem, its physical coherence, and the constitutive properties of the material under consideration derive directly from the integral kernel. In the following, we investigate the properties of the integral kernel $\mathbf{f}(\mathbf{x}'-\mathbf{x},\mathbf{u}(\mathbf{x}')-\mathbf{u}(x))$ and decipher its relation with the behavior of the material. The peridynamics integral kernel is shaped up by the nature of internal forces, and, indeed, some physical constraints are required. With the intent to ease the notation, we define the following quantities (see Fig. 2b): $\boldsymbol{\xi}:=\mathbf{x}'-\mathbf{x}$ and $\boldsymbol{\eta}:=\mathbf{u}(\mathbf{x}')-\mathbf{u}(\mathbf{x})$, so that $\mathbf{f}(\mathbf{x}'-\mathbf{x},\mathbf{u}(\mathbf{x}')-\mathbf{u}(\mathbf{x}))\equiv\mathbf{f}(\boldsymbol{\xi},\boldsymbol{\eta})$.

- *Actio et reactio principle*:

$$\forall \mathbf{x}, \mathbf{x}' \in B_\delta(\mathbf{x}): \quad \mathbf{f}(-\boldsymbol{\xi}, -\boldsymbol{\eta}) = -\mathbf{f}(\boldsymbol{\xi}, \boldsymbol{\eta}). \tag{2.6}$$

The actio et reactio principle, i.e., the *third law of Newton*, ensures the conservation of linear momentum of the system composed of mutually interacting particles.

- *Angular momentum conservation*:

$$\forall \mathbf{x}, \mathbf{x}' \in B_\delta(\mathbf{x}): \quad (\boldsymbol{\xi} + \boldsymbol{\eta}) \times \mathbf{f}(\boldsymbol{\xi}, \boldsymbol{\eta}) = \mathbf{0}, \tag{2.7}$$

that is, the relative deformed ray-vector connecting $\mathbf{x}$ and $\mathbf{x}'$ is $(\boldsymbol{\xi} + \boldsymbol{\eta})$. This condition is satisfied if and only if the pairwise force density vector has the same direction as the relative deformed ray vector,

$$\mathbf{f}(\boldsymbol{\xi}, \boldsymbol{\eta}) = f(\boldsymbol{\xi}, \boldsymbol{\eta})(\boldsymbol{\xi} + \boldsymbol{\eta}), \quad \forall \boldsymbol{\xi}, \boldsymbol{\eta}, \tag{2.8}$$

with a scalar-valued function $f(\boldsymbol{\xi}, \boldsymbol{\eta})$.

- *Hyperelastic material*: hyperelastic is the attribute given to a material such that

$$\int_\Gamma \mathbf{f}(\boldsymbol{\xi}, \boldsymbol{\eta}) \cdot d\boldsymbol{\eta} = 0 \quad \forall \text{ closed curves } \Gamma, \forall \boldsymbol{\xi} \neq \mathbf{0}, \tag{2.9}$$

or, equivalently, by Stokes' theorem

$$\nabla_\eta \times \mathbf{f}(\boldsymbol{\xi}, \boldsymbol{\eta}) = \mathbf{0} \quad \forall \boldsymbol{\xi}, \boldsymbol{\eta}, \tag{2.10}$$

and, consequently,

$$\mathbf{f}(\boldsymbol{\xi}, \boldsymbol{\eta}) = \nabla_\eta \Phi(\boldsymbol{\xi}, \boldsymbol{\eta}) \quad \forall \boldsymbol{\xi}, \boldsymbol{\eta}, \tag{2.11}$$

where $\Phi(\boldsymbol{\xi}, \boldsymbol{\eta})$ is a scalar-valued potential function in $C^2(\mathbb{R}^n \setminus \{\mathbf{0}\} \times \mathbb{R}^n)$ [1]. Since the pairwise force must satisfy the angular momentum conservation, we obtain the following condition on the scalar-valued function $f(\boldsymbol{\xi}, \boldsymbol{\eta})$:

$$\frac{\partial f(\boldsymbol{\xi}, \boldsymbol{\eta})}{\partial \boldsymbol{\eta}} = g(\boldsymbol{\xi}, \boldsymbol{\eta})(\boldsymbol{\xi} + \boldsymbol{\eta}). \tag{2.12}$$

Integrating both sides of the equation, we get the following condition on $g(\boldsymbol{\xi}, \boldsymbol{\eta})$ [1]:

$$\mathbf{f}(\boldsymbol{\xi}, \boldsymbol{\eta}) = h\big(|\boldsymbol{\xi} + \boldsymbol{\eta}|, \boldsymbol{\xi}\big)(\boldsymbol{\xi} + \boldsymbol{\eta}) \tag{2.13}$$

for a scalar valued function $h(|\boldsymbol{\xi} + \boldsymbol{\eta}|, \boldsymbol{\xi})$. From (2.13) the elastic nature of $\mathbf{f}$ can be clearly observed; in fact, the interaction force depends only on the initial relative position between points $\mathbf{x}$ and $\mathbf{x}'$ and the modulus of their relative position in the deformed configuration Ω_t at time t, $|\boldsymbol{\xi} + \boldsymbol{\eta}|$. Under the *isotropy* hypothesis, the general dependence on vector $\boldsymbol{\xi}$ can be substituted with a dependence on $|\boldsymbol{\xi}|$:

$$\mathbf{f}(\boldsymbol{\xi}, \boldsymbol{\eta}) = h\big(|\boldsymbol{\xi} + \boldsymbol{\eta}|, |\boldsymbol{\xi}|\big)(\boldsymbol{\xi} + \boldsymbol{\eta}). \tag{2.14}$$

Thus the bond forces can be considered as modeling a spring network that connects each point $\mathbf{x} \in \Omega_0$ pairwise with $\mathbf{x}' \in B_\delta(\mathbf{x}) \cap \Omega_0$.

- *Linear elastic material*: if $|\boldsymbol{\eta}| \ll 0$, then the peridynamic kernel can be linearized around $\boldsymbol{\eta} = \mathbf{0}$ so that

$$\mathbf{f}(\boldsymbol{\xi}, \boldsymbol{\eta}) \approx \mathbf{f}(\boldsymbol{\xi}, \mathbf{0}) + \left.\frac{\partial \mathbf{f}(\boldsymbol{\xi}, \boldsymbol{\eta})}{\partial \boldsymbol{\eta}}\right|_{\boldsymbol{\eta}=\mathbf{0}} \boldsymbol{\eta}; \tag{2.15}$$

a second-order *micromodulus tensor* can be defined as

$$\boldsymbol{C}(\boldsymbol{\xi}) = \left.\frac{\partial \mathbf{f}(\boldsymbol{\xi}, \boldsymbol{\eta})}{\partial \boldsymbol{\eta}}\right|_{\boldsymbol{\eta}=\mathbf{0}} = \boldsymbol{\xi} \otimes \left.\frac{\partial f(\boldsymbol{\xi}, \boldsymbol{\eta})}{\partial \boldsymbol{\eta}}\right|_{\boldsymbol{\eta}=\mathbf{0}} + f_0, \tag{2.16}$$

where, to simplify the notation, $f_0 = f(\boldsymbol{\xi}, \mathbf{0})$. After an application of linear momentum balance (2.6), elasticity (2.10), and isotropy condition, the micromodulus tensor can be expressed in the form [1]

$$\boldsymbol{C}(\boldsymbol{\xi}) = \lambda\big(|\boldsymbol{\xi}|\big)\boldsymbol{\xi} \otimes \boldsymbol{\xi} + f_0. \tag{2.17}$$

Thus, for a linearized hyperelastic material, its peridynamic kernel shows the following structure:

$$\mathbf{f}(\boldsymbol{\xi}, \boldsymbol{\eta}) = \mathbf{f}(\boldsymbol{\xi}, \mathbf{0}) + \big(\lambda\big(|\boldsymbol{\xi}|\big)\boldsymbol{\xi} \otimes \boldsymbol{\xi} + f_0\big)\boldsymbol{\eta}. \tag{2.18}$$

3 Peridynamic models for hyperelastic materials

Looking at the literature regarding peridynamic elastic theory, different integral kernel (i.e., pairwise force $\mathbf{f}(\boldsymbol{\xi}, \boldsymbol{\eta})$) structures can be found; in the following, a survey of various employed expressions for peridynamic kernels is detailed. For all the listed models, the pairwise force $\mathbf{f}(\boldsymbol{\xi}, \boldsymbol{\eta})$ vanishes for $|\boldsymbol{\xi}| > \delta$; such a condition on $\mathbf{f}$, even if not explicitly stated, must be considered to hold. In [1] a simple model for three-dimensional microelastic isotropic peridynamic material subject to antiplane shear is proposed to predict the onset of fractures:

$$\mathbf{f}(\boldsymbol{\eta}, \boldsymbol{\xi}) = \begin{cases} c\frac{|\boldsymbol{\xi}+\boldsymbol{\eta}|-|\boldsymbol{\xi}|}{|\boldsymbol{\xi}+\boldsymbol{\eta}|}(\boldsymbol{\xi} + \boldsymbol{\eta}) & \text{if } |\boldsymbol{\xi} + \boldsymbol{\eta}| - |\boldsymbol{\xi}| \le u \text{ and } |\boldsymbol{\xi}| \le \delta, \\ \mathbf{0} & \text{otherwise,} \end{cases} \tag{3.1}$$

where c is a constant depending on the material, and u_* is a parameter such that if the displacement of the relative point in the deformed configuration exceeds the threshold level u_*, then the associated bond is broken, and fracture can emerge. Another model proposed in [1] for isotropic microelastic peridynamic materials is described by the potential function

$$\Phi\big(|\boldsymbol{\xi} + \boldsymbol{\eta}|, |\boldsymbol{\xi}|\big) = \alpha\big(|\boldsymbol{\xi}|\big)\big(|\boldsymbol{\xi} + \boldsymbol{\eta}|^2 - |\boldsymbol{\xi}|^2\big)^2, \tag{3.2}$$

so that

$$\mathbf{f}(\boldsymbol{\eta}, \boldsymbol{\xi}) = a\big(|\boldsymbol{\xi}|\big)\big(|\boldsymbol{\xi} + \boldsymbol{\eta}|^2 - |\boldsymbol{\xi}|^2\big)(\boldsymbol{\xi} + \boldsymbol{\eta}), \tag{3.3}$$

where $a(|\boldsymbol{\xi}|)$ is a scalar function.

In [49] a peridynamic kernel for the so-called *prototype microelastic brittle* (PMB) material is proposed; the pairwise force for an isotropic PMB material is conceived as linearly proportional to the finite stretch $s := (|\boldsymbol{\xi} + \boldsymbol{\eta}| - |\boldsymbol{\xi}|)/|\boldsymbol{\xi}|$, so that

$$\mathbf{f}(\boldsymbol{\eta}, \boldsymbol{\xi}) = f\big(|\boldsymbol{\xi} + \boldsymbol{\eta}|, |\boldsymbol{\xi}|\big)\boldsymbol{n}, \tag{3.4}$$

where $\boldsymbol{n} := (\boldsymbol{\xi} + \boldsymbol{\eta})/|\boldsymbol{\xi} + \boldsymbol{\eta}|$, and the scalar function f is defined as follows:

$$f = cs\mu(s,t) = c\frac{|\boldsymbol{\xi} + \boldsymbol{\eta}| - |\boldsymbol{\xi}|}{|\boldsymbol{\xi}|}\mu(s,t) \tag{3.5}$$

with

$$\mu(s,t) = \begin{cases} 1 & \text{if } s(t', \boldsymbol{\xi}) < s_0, \\ 0 & \text{otherwise,} \end{cases} \qquad \text{for all } 0 \le t' \le t; \tag{3.6}$$

c is the *micromodulus constant*, and $\mu(s,t)$ is a function that records if at a certain time $t' \le t$, the bond stretch s associated with the pair $(\mathbf{x}, \mathbf{x}')$ has exceeded the critical value s_0: if so, then the bond is considered *broken*, and a zero-valued pairwise force is assigned for all $t \ge t'$. By comparing the strain energy density value obtained under isotropic extension with peridynamics and classical continuum theory the following value of c is readily found [49]:

$$c = \frac{18k}{\pi\delta^4}, \tag{3.7}$$

where k is the material bulk modulus. Over time, following the same approach as in [28], for the microconductivity function, the micromodulus constant c has been generalized to $c(\boldsymbol{\xi}, \delta)$, i.e., to a *micromodulus function*, to describe in more detail how pairwise force intensity distributes over the peridynamic horizon $B_\delta(\mathbf{x})$; intuitively, the force intensity decreases as the distance between $\mathbf{x}$ and $\mathbf{x}' \in B_\delta(\mathbf{x})$ increases, but it can do it in various ways. The micromodulus function is defined as

$$c(\boldsymbol{\xi}, \delta) := c(\mathbf{0}, \delta)k(\boldsymbol{\xi}, \delta), \tag{3.8}$$

where $c(\mathbf{0}, \delta)$ is a constant obtained by comparing peridynamic strain density with the classical mechanical theories [73], and $k(\boldsymbol{\xi}, \delta)$ is a function defined on Ω_0 such that (to meet the momentum conservation and isotropy conditions) [77]

$$\begin{cases} k(\boldsymbol{\xi}, \delta) = k(-\boldsymbol{\xi}, \delta), \\ \lim_{\boldsymbol{\xi}\to\mathbf{0}} k(\boldsymbol{\xi}, \delta) = \max_{\boldsymbol{\xi}\in\mathbb{R}^n}\{k(\boldsymbol{\xi}, \delta)\}, \\ \lim_{\boldsymbol{\xi}\to\delta} k(\boldsymbol{\xi}, \delta) = 0, \\ \int_{\mathbb{R}^n} \lim_{\delta\to 0} k(\boldsymbol{\xi}, \delta)\, d\mathbf{x} = \int_{\mathbb{R}^n} \Delta(\boldsymbol{\xi})\, d\mathbf{x} = 1, \end{cases} \tag{3.9}$$

where $\Delta(\boldsymbol{\xi})$ is the Dirac delta function. The simplest adopted form for the micromodulus function is $c(\mathbf{0}, \delta)k(\boldsymbol{\xi}, \delta) = c\mathbf{1}_{B_\delta(\mathbf{x}')}$, where $\mathbf{1}_A : X \to \mathbb{R}$ is the indicator function for a subset

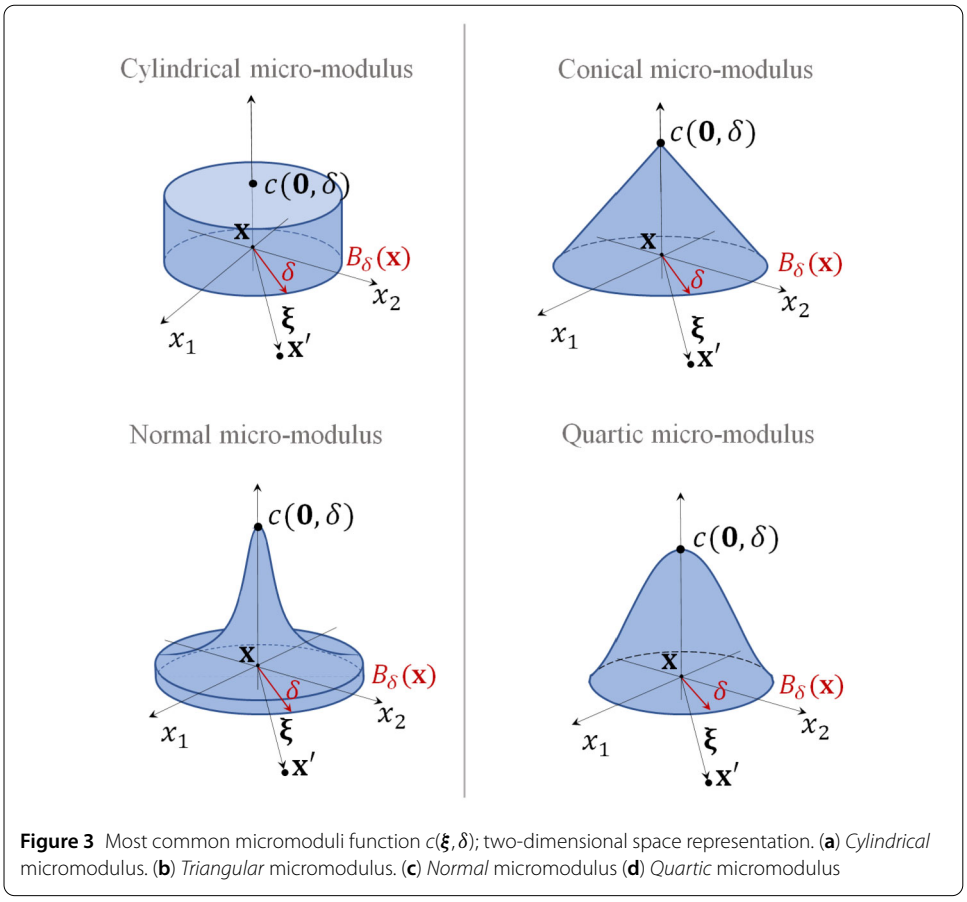

Figure 3 Most common micromoduli function $c(\boldsymbol{\xi},\delta)$; two-dimensional space representation. (**a**) *Cylindrical* micromodulus. (**b**) *Triangular* micromodulus. (**c**) *Normal* micromodulus (**d**) *Quartic* micromodulus

$A \subset X$, i.e.,

$$\mathbf{1}_A(x) := \begin{cases} 1, & x \in A, \\ 0, & x \notin A. \end{cases} \tag{3.10}$$

this kind of micromodulus function, referred as *cylindrical* (see Fig. 3a), corresponds to the peridynamic kernel in (3.4). In [7] a *triangular* micromodulus function (see Fig. 3b) is introduced, characterized by a linear function $k(\boldsymbol{\xi},\delta)$ of the following type:

$$k(\boldsymbol{\xi},\delta) = \left(1 - \frac{|\boldsymbol{\xi}|}{\delta}\right)\mathbf{1}_{B_\delta(\mathbf{x}')}. \tag{3.11}$$

Since the most common discrete physical systems are characterized by a Maxwell–Boltzmann distribution, to include this behavior in peridynamics, a *normal* micromodulus function (see Fig. 3c)

$$k(\boldsymbol{\xi},\delta) = e^{-(|\boldsymbol{\xi}|/\delta)^2}\mathbf{1}_{B_\delta(\mathbf{x}')}, \tag{3.12}$$

is proposed in [74], whereas in [77] a *quartic polynomial* micromodulus function

$$k(\boldsymbol{\xi},\delta) = \left(1 - \left(\frac{\xi}{\delta}\right)^2\right)^2 \mathbf{1}_{B_\delta(\mathbf{x}')} \tag{3.13}$$

(see Fig. 3d) is proposed. Therefore peridynamic kernels like those proposed in [7, 49, 77], and [74] can be included in a generalized prototype microelastic brittle (PMB) material kernel characterized by the form

$$\mathbf{f}(\boldsymbol{\xi},\boldsymbol{\eta}) = c(\boldsymbol{\xi},\delta)\underbrace{\frac{|\boldsymbol{\xi}+\boldsymbol{\eta}|-|\boldsymbol{\xi}|}{|\boldsymbol{\xi}|}}_{s}\mu(s,t). \tag{3.14}$$

An interesting survey and analysis of the effects of different micromodulus functions on fracture development can be found in [73]. In [72], peridynamic kernels for failure analysis of material nanostructures are presented: a pairwise force model is proposed for an isotropic Blatz–Ko rubbery membrane and fiber materials characterized by van der Waals interactions, respectively,

$$\mathbf{f}(\boldsymbol{\xi},\boldsymbol{\eta}) = \frac{2c}{|\boldsymbol{\xi}|}\left(\frac{|\boldsymbol{\xi}+\boldsymbol{\eta}|}{|\boldsymbol{\xi}|}-\left(\frac{|\boldsymbol{\xi}+\boldsymbol{\eta}|}{|\boldsymbol{\xi}|}\right)^{-3}\right)g\big(|\boldsymbol{\xi}|\big)\mu\big(|\boldsymbol{\xi}+\boldsymbol{\eta}|,t\big)\mathbf{n} \tag{3.15}$$

and

$$\begin{aligned}\mathbf{f}(\boldsymbol{\xi},\boldsymbol{\eta}) = {}& \left[\frac{2c}{|\boldsymbol{\xi}|}\left(\frac{|\boldsymbol{\xi}+\boldsymbol{\eta}|}{|\boldsymbol{\xi}|}-\left(\frac{|\boldsymbol{\xi}+\boldsymbol{\eta}|}{|\boldsymbol{\xi}|}\right)^{-3}\right)\right]g\big(|\boldsymbol{\xi}|\big)\mu\big(|\boldsymbol{\xi}+\boldsymbol{\eta}|,t\big)\\ & -\frac{12\alpha}{\delta}\left(\frac{\delta}{|\boldsymbol{\xi}+\boldsymbol{\eta}|}\right)^{13}+\frac{6\beta}{\delta}\left(\frac{\delta}{|\boldsymbol{\xi}+\boldsymbol{\eta}|}\right)^{7}\mathbf{n},\end{aligned} \tag{3.16}$$

where α, β, c are constants, and $g(|\boldsymbol{\xi}|)$ is a continuous function that takes into account the possibility of different elastic responses for different characteristic bond lengths. In [75] the peridynamic elastic material is thought as composed of a superposition of elastic rods with elastic micromodulus function $c(\boldsymbol{\xi},\delta)$ that connects pairwise each point belonging to the body. Starting from Newton's second law applied to each rod connecting the point $\mathbf{x}$ with its family, we obtain the following constructive integral kernel:

$$\mathbf{f}(\boldsymbol{\eta},\boldsymbol{\xi}) = c(\boldsymbol{\xi},\delta)\frac{|\boldsymbol{\xi}+\boldsymbol{\eta}|-|\boldsymbol{\xi}|}{|\boldsymbol{\xi}|^2}\boldsymbol{n}. \tag{3.17}$$

In [43, 46], where one- and two-dimensional nonlinear elastic materials have been considered in the development of a numerical approximation method for the resolution of the peridynamic problem, the following integral kernel structure of convolution type is proposed:

$$\mathbf{f}(\boldsymbol{\xi},\boldsymbol{\eta}) = C(\boldsymbol{\xi})w(\boldsymbol{\xi}+\boldsymbol{\eta}); \tag{3.18}$$

the micromodulus function $C(\boldsymbol{\xi})$ is even, whereas $w(\boldsymbol{\xi}+\boldsymbol{\eta})$ is odd, and both are global Lipschitz continuous functions; specifically, the authors choose $w(\boldsymbol{\xi}+\boldsymbol{\eta}) = (\boldsymbol{\xi}+\boldsymbol{\eta})^r$, where $r > 1$ is an odd number. The peridynamic kernel results as follows:

$$\mathbf{f}(\boldsymbol{\xi},\boldsymbol{\eta}) = C(\boldsymbol{\xi})(\boldsymbol{\xi}+\boldsymbol{\eta})^r. \tag{3.19}$$

In [78] and [79] the following nonlinear peridynamic integral kernel in $\mathbb{R}^n$ for an hyperelastic material is considered by establishing the nonlinear elastic potential function

$$\Phi(\boldsymbol{\xi},\boldsymbol{\eta}) = \kappa \frac{|\boldsymbol{\xi}+\boldsymbol{\eta}|^p}{|\boldsymbol{\xi}|^{n+\alpha p}} + \Psi(\boldsymbol{\xi},\boldsymbol{\eta}), \tag{3.20}$$

where n is the space dimension (practically, $n \in \{1,2,3\}$), p and α real numbers such that

$$p \geq 2, \quad \alpha \in (0,1), \tag{3.21}$$

and $\Psi(\boldsymbol{\xi},\boldsymbol{\eta})$ is a sufficiently smooth perturbation function. Considering that $\mathbf{f} = \nabla_{\boldsymbol{\eta}}\Phi$ for hyperelastic materials, the following structure for the constitutive pairwise force is obtained:

$$\mathbf{f}(\boldsymbol{\xi},\boldsymbol{\eta}) = \kappa p \frac{|\boldsymbol{\eta}+\boldsymbol{\xi}|^{p-2}}{|\boldsymbol{\xi}|^{N+\alpha p}}(\boldsymbol{\eta}+\boldsymbol{\xi}) + \psi(\boldsymbol{\xi},\boldsymbol{\eta}). \tag{3.22}$$

It is worth noting that for this expression and in general for all pairwise forces defined by an elastic potential function such that

$$\int_{\mathbb{R}^N}\int_{B_\delta(\mathbf{0})} \Phi\big(\boldsymbol{\xi}, \mathbf{u}_0(\mathbf{x}) - \mathbf{u}_0\big(\mathbf{x}'\big)\big)\, d\mathbf{x}\, d\boldsymbol{\xi} < \infty \tag{3.23}$$

and $\mathbf{u}_0, \mathbf{v}_0 \in L^2(\mathbb{R}^N;\mathbb{R}^N)$, the associated Cauchy problem in (2.4) admits a unique, stable, and energy-bounded weak solution, so that the peridynamic equation is well posed; for a detailed treatment and rigorous proofs of the aforementioned well-posedness of such type of peridynamic models, see [78].

Then after neglecting minor differences, the pairwise force models listed below could be thought as representatives of the peridynamic kernel structures commonly adopted in literature for the modeling of hyperelastic materials. An interesting feature of the listed models is that even though each of them ensures compliance with the basic mechanical principle, i.e., conservation of linear and angular momentum, rather different structures of the peridynamic kernel are employed, so that it appears surely intriguing to analyze both main shared features and differences between such different models.

4 Features of kernel structure

4.1 Nonlocality

As stated earlier, the key feature of peridynamics is nonlocality. In the previous section, the role of nonlocality has been highlighted by the fact that internal forces acting at a point $\mathbf{x}$ at every time t are determined by a process of integration over a *finite* region; but differences between the classical (local) theory of continua and peridynamics may be emphasized within the framework of a more fundamental subject, kinematics. The crucial difference between classical mechanics and peridynamics relies on the role of $\nabla_{\mathbf{x}}\mathbf{u}$ on the motion of points. Given the displacement function $\mathbf{u}(\mathbf{x},t)$, we get that the deformed position of a point in Ω_0 is described by the motion mapping $(\mathbf{x}+\mathbf{u}(\cdot,t))$ that maps points in the reference space to points in the geometrical space; the schism between classical local theory and peridynamics involves the Taylor expansion of the motion of a so-called *undeformed fiber* $\mathbf{x}+\ell\boldsymbol{e_R}$ [80], where ℓ is the length of the fiber, and $\boldsymbol{e_R}$ is a unitary vector in

Ω_0 representing the fiber direction. Let $\mathbf{x}'$ be a point in Ω_0 individuated by a undeformed fiber, that is, $\mathbf{x}' := \mathbf{x} + \ell(\boldsymbol{e_R})$. After performing a Taylor expansion of the motion of the fiber with respect to the base point $\mathbf{x}$, we obtain the following expression:

$$\mathbf{y}' - \mathbf{y} = \big[\boldsymbol{I} + \nabla_{\mathbf{x}}\mathbf{u}(\mathbf{x})\big](\mathbf{x}' - \mathbf{x}) + \mathrm{o}\big(|\mathbf{x}' - \mathbf{x}|\big), \tag{4.1}$$

where

$$\big[\nabla_{\mathbf{x}}\mathbf{u}(\mathbf{x})\big]_{i,j} := \frac{\partial u(\mathbf{x})_i}{\partial x_j}, \tag{4.2}$$

$\mathbf{y}' := \mathbf{y} + \boldsymbol{e}$ (with $\boldsymbol{e}$ being, in general, nonunitary) represents the corresponding *deformed fiber* in Ω_t, and $\boldsymbol{I}$ is the identity matrix. Considering the limit case $\ell \to 0$, the transformation law from an undeformed fiber into a deformed fiber results in [80] (see Fig. 4a)

$$\boldsymbol{e} = \mathbf{y}' - \mathbf{y} = \ell\big(\big[\boldsymbol{I} + \nabla_{\mathbf{x}}\mathbf{u}(\mathbf{x})\big]\boldsymbol{e_R}\big) + \mathrm{o}(\ell) \approx \ell\big(\big[(\boldsymbol{I} + \nabla_{\mathbf{x}}\mathbf{u})\mathbf{x}\big]\boldsymbol{e_R}\big), \tag{4.3}$$

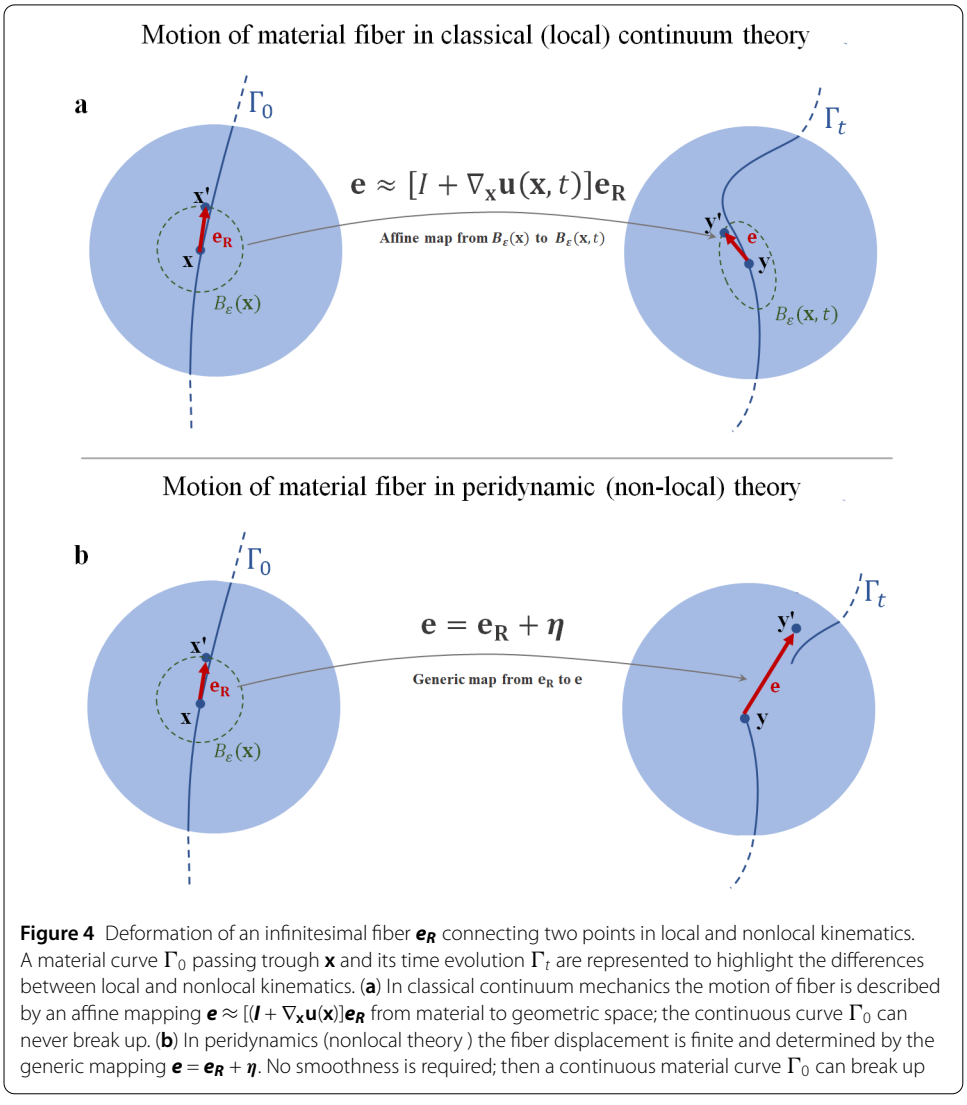

Figure 4 Deformation of an infinitesimal fiber $\boldsymbol{e_R}$ connecting two points in local and nonlocal kinematics. A material curve Γ_0 passing trough $\mathbf{x}$ and its time evolution Γ_t are represented to highlight the differences between local and nonlocal kinematics. (**a**) In classical continuum mechanics the motion of fiber is described by an affine mapping $\boldsymbol{e} \approx [(\boldsymbol{I} + \nabla_{\mathbf{x}}\mathbf{u}(\mathbf{x})]\boldsymbol{e_R}$ from material to geometric space; the continuous curve Γ_0 can never break up. (**b**) In peridynamics (nonlocal theory) the fiber displacement is finite and determined by the generic mapping $\boldsymbol{e} = \boldsymbol{e_R} + \boldsymbol{\eta}$. No smoothness is required; then a continuous material curve Γ_0 can break up

where time dependence of $\mathbf{u}$ has been omitted; transformation laws for surfaces and volumes in Ω_0 are obtained similarly. Given a unitary length of undeformed fiber ($\ell = 1$), so that

$$\boldsymbol{e} \approx \big[(\boldsymbol{I} + \nabla_{\mathbf{x}}\mathbf{u}(\mathbf{x})\big]\boldsymbol{e_R}, \tag{4.4}$$

its stretching can be defined, as usual, by $s := |\boldsymbol{e}|/|\boldsymbol{e_R}|$, and therefore

$$\begin{aligned} s := \frac{|\boldsymbol{e}|}{|\boldsymbol{e_R}|} = \frac{\boldsymbol{e}\cdot\boldsymbol{e}}{1} &= (\boldsymbol{e_R} + \nabla_{\mathbf{x}}\mathbf{u}\boldsymbol{e_R})\cdot(\boldsymbol{e_R} + \nabla_{\mathbf{x}}\mathbf{u}\boldsymbol{e_R}) \\ &= \underbrace{1 + \nabla_{\mathbf{x}}\mathbf{u}\boldsymbol{e_R}\cdot\boldsymbol{e_R} + \nabla_{\mathbf{x}}\mathbf{u}^{\top}\boldsymbol{e_R}\cdot\boldsymbol{e_R}}_{\text{linear stretch}} + \underbrace{\nabla_{\mathbf{x}}\mathbf{u}^{\top}\nabla_{\mathbf{x}}\mathbf{u}\boldsymbol{e_R}\cdot\boldsymbol{e_R}}_{\text{nonlinear stretch}}. \end{aligned} \tag{4.5}$$

Note that the stretch of the fiber is clearly governed only by local measures. Since elastic forces are in direct relationship with the stretch, it follows that the dynamical evolutionary problem is governed by local concepts. Therefore in classical continuum mechanics, material body kinematics relies on assuming the existence of $\nabla_{\mathbf{x}}\mathbf{u}$ on Ω_t for every time $t \in [0, +\infty)$, so that a Taylor expansion for the motion at every point in the body can be performed. In such a way, kinematics of $\mathbf{x}$ and its neighborhood are defined by an affine mapping between reference and spatial points, defined by $\nabla_{\mathbf{x}}\mathbf{u}$. In short, the limits of classical mechanics stem directly from the requirement that the motion of a material body must be described by a continuous-time sequence of differentiable manifolds. Looking at peridynamics elasticity theory, it is prominent that $\nabla_{\mathbf{x}}\mathbf{u}$ does not play any role in the description of motion of points, so that the stretch of a fiber is purely described by a finite (nonlocal) and generally nonlinear quantity, the bond stretch $s = |\boldsymbol{\xi} + \boldsymbol{\eta}|/|\boldsymbol{\xi}|$. Looking at the peridynamics models listed above, we can see that all pairwise forces are functions of bonds stretch, i.e., can be expressed as

$$\mathbf{f}(\boldsymbol{\xi}, \boldsymbol{\eta}) = h\big(|\boldsymbol{\xi} + \boldsymbol{\eta}|, |\boldsymbol{\xi}|\big)(\boldsymbol{\xi} + \boldsymbol{\eta}) = \tilde{h}(s)(\boldsymbol{\xi} + \boldsymbol{\eta}), \tag{4.6}$$

so that from a finite (nonlocal) definition of fiber stretching (see Fig. 4b) a nonlocal dynamics follows for every reference point in Ω_0. No prescriptions are imposed on the displacement function $\mathbf{u}(\mathbf{x}, t)$, and, consequently, the motion of the material body can be described by nondifferentiable or even discontinuous mapping (with respect to the space variable); obviously, such mathematical freedom is reflected by the variety of peridynamic kernels adopted in the literature.

4.2 Impenetrability of matter principle

From the mathematical freedom allowed in peridynamics, various types of integral kernels emerge, sharing, however, a common structure: each model falls into the class of rational functions of variables $\boldsymbol{\xi} + \boldsymbol{\eta}$ and $\boldsymbol{\xi}$ (the micromodulus function structure $c(\boldsymbol{\xi}, \delta)$, which can be quite general, can be neglected in this classification because its structure makes it irrelevant in the following discussion on singularities and impenetrability of matter). In the following, we will briefly discuss certain features derived from the presence of the denominator with respect to a fundamental physical principle, the impenetrability of matter. To be physically consistent, the defined peridynamic kernel $\mathbf{f}(\boldsymbol{\xi}, \boldsymbol{\eta})$ must necessarily respond

to the basic principle of the impenetrability of matter, that is, two material bodies cannot occupy the same position at the same time. In classical continuum theory the condition of impenetrability is imposed via kinematics constrain on $J := \det(\nabla_{\mathbf{x}} \chi_t)$, where χ_t is the deformation function ($\chi_t := \mathbf{x} + \mathbf{u}(\mathbf{x}, t)$) such that $J > 0$. Noting that in classical continuum mechanics $\mathbf{u}(\mathbf{x}, t)$ is assumed to be a smooth function (so that $\nabla_{\mathbf{x}} \chi$ is continuous) and considering that $J = 1$ in the reference configuration, the kinematic constrain $J > 0$ implies the impossibility for every volume element Δv belonging to Ω_0 (which is individuated by a vector basis) to change its orientation with time. Indeed, by continuity it would imply that at a certain $t = \tau$, $J = 0$, i.e., Δv collapses into a plane (or a line), so that points in the volume have been compenetrated. The same reasoning is analogous for a surface element Δs. Obviously, for peridynamics theory, this type of constraint has no meaning. From a different perspective, impenetrability condition is granted by the functional form of $\Phi(\mathbf{x}' - \mathbf{x}, \mathbf{u}(\mathbf{x}', t) - \mathbf{u}(\mathbf{x}, t))$ (see Eq. (3.20)), or better, by the choice of its singular kernel. Hence at any time t, the energy $E[\mathbf{u}](t)$ associated with Ω_t, given by

$$E[\mathbf{u}](t) := \frac{\|\mathbf{u}_t(\cdot, t)\|^2_{L^2(\Omega_t)}}{2} + \frac{1}{2} \int_{\Omega_t} \int_{B_\delta(\mathbf{x})} \Phi\big(\mathbf{x}' - \mathbf{x}, \mathbf{u}\big(\mathbf{x}', t\big) - \mathbf{u}(\mathbf{x}, t)\big)\, d\mathbf{x}'\, d\mathbf{x}, \tag{4.7}$$

satisfies

$$\forall \mathbf{x}, \tilde{\mathbf{x}} \in \Omega_0, \quad |\mathbf{x} - \tilde{\mathbf{x}}| \to 0 \quad \Rightarrow \quad E[\mathbf{u}](t) \to \infty. \tag{4.8}$$

Therefore a physical configuration where two points penetrate each other is energetically inaccessible. Looking at the expression for $E[\mathbf{u}](t)$ and given the finiteness of the velocity $\partial_t \mathbf{u}$ of points, the energetic condition of impenetrability relies upon the structure of the elastic potential Φ (which in turn determines the peridynamic kernel structure). A necessary condition for impenetrability is the possibility of the integral terms $\int_{B_\delta(\mathbf{x})} \Phi(\boldsymbol{\xi}, \boldsymbol{\eta})\, d\mathbf{x}'$ to be singular. Looking at Table 1, we can notice that the only source of singularity is the presence of denominator of type $|\boldsymbol{\xi}|^\beta$ for some $\beta > 0$; in fact, $|\boldsymbol{\xi}|^\beta \to 0$ during the integration process over $B_\delta(\mathbf{x})$. Consequently, integral kernels as in (3.1), (3.3), and (3.19) can never reach a singular value. Focusing on the integral kernel (3.22), which is the most general model (including both linear and nonlinear material behavior) for which the well-posedness of the peridynamic equation has been proven, the energetic version of the impenetrability condition seems to be suitable; in fact, solutions of this model satisfy the following energetic condition [78]:

$$E[\mathbf{u}](t) \leq E[\mathbf{u}](0) \quad \text{for a.e. } t \geq 0, \tag{4.9}$$

so that, given a configuration with finite energy, all motions that imply compenetration are naturally excluded. The possibility for the elastic potential function of reaching a singular value as a result of the integration over $B_\delta(\mathbf{x})$ is a *necessary but insufficient* condition for impenetrability, and a closer investigation is necessary to prove that condition (4.8) holds for the considered peridynamic kernel. It is interesting to highlight that such a singularity condition for $\int_{B_\delta(\mathbf{x})} \Phi(\boldsymbol{\xi}, \boldsymbol{\eta})\, d\mathbf{x}'$ does not hold when the integration process is carried out by numerical quadrature methods; in fact, $|\boldsymbol{\xi}|$ is a mesh-dependent quantity and is always a finite number. The conciliation of such a discrepancy between continuum and discrete

Table 1 List of adopted integral kernels and the corresponding elastic potential (the function $\mu(s,t)$ has been omitted from the model corresponding to (3.14) because it is negligible in the current context); the models in (3.15) and (3.16) are not in the table because of readability

Equation	$\Phi(\boldsymbol{\xi},\boldsymbol{\eta})$	Equation	$\mathbf{f}(\boldsymbol{\xi},\boldsymbol{\eta})$
	$\frac{c}{2}(\lvert\boldsymbol{\xi}+\boldsymbol{\eta}\rvert-\lvert\boldsymbol{\xi}\rvert)^2$	(3.1)	$c(\lvert\boldsymbol{\xi}+\boldsymbol{\eta}\rvert-\lvert\boldsymbol{\xi}\rvert)\boldsymbol{n}$
(3.2)	$\alpha(\lvert\boldsymbol{\xi}\rvert)(\lvert\boldsymbol{\xi}+\boldsymbol{\eta}\rvert^2-\lvert\boldsymbol{\xi}\rvert^2)^2$,	(3.3)	$a(\lvert\boldsymbol{\xi}\rvert)(\lvert\boldsymbol{\xi}+\boldsymbol{\eta}\rvert^2-\lvert\boldsymbol{\xi}\rvert^2)(\boldsymbol{\xi}+\boldsymbol{\eta})$
	$c(\boldsymbol{\xi},\delta)\frac{(\lvert\boldsymbol{\xi}+\boldsymbol{\eta}\rvert-\lvert\boldsymbol{\xi}\rvert)^2}{2\lvert\boldsymbol{\xi}\rvert}$	(3.14)	$c(\boldsymbol{\xi},\delta)\frac{\lvert\boldsymbol{\xi}+\boldsymbol{\eta}\rvert-\lvert\boldsymbol{\xi}\rvert}{\lvert\boldsymbol{\xi}\rvert}\boldsymbol{n}$
	$c(\boldsymbol{\xi},\delta)\frac{(\lvert\boldsymbol{\xi}+\boldsymbol{\eta}\rvert-\lvert\boldsymbol{\xi}\rvert)^2}{2\lvert\boldsymbol{\xi}\rvert^2}$	(3.17)	$c(\boldsymbol{\xi},\delta)\frac{\lvert\boldsymbol{\xi}+\boldsymbol{\eta}\rvert-\lvert\boldsymbol{\xi}\rvert}{\lvert\boldsymbol{\xi}\rvert^2}\boldsymbol{n}$
	$\frac{C(\boldsymbol{\xi})}{r+1}(\boldsymbol{\xi}+\boldsymbol{\eta})^{r+1}$	(3.19)	$C(\boldsymbol{\xi})(\boldsymbol{\xi}+\boldsymbol{\eta})^r$
(3.20)	$\kappa\frac{\lvert\boldsymbol{\xi}+\boldsymbol{\eta}\rvert^p}{\lvert\boldsymbol{\xi}\rvert^{N+\alpha p}}+\Psi(\boldsymbol{\xi},\boldsymbol{\eta})$	(3.22)	$\kappa p\frac{\lvert\boldsymbol{\eta}+\boldsymbol{\xi}\rvert^{p-2}}{\lvert\boldsymbol{\xi}\rvert^{N+\alpha p}}(\boldsymbol{\eta}+\boldsymbol{\xi})+\psi(\boldsymbol{\xi},\boldsymbol{\eta})$

peridynamic theories, without the trivial solution of indefinitely increasing mesh density (which is obviously unfeasible), would be surely an interesting research topic.

4.3 Nonlinearities and fractures

What clearly distinguishes up peridynamic kernels listed in Table 1 is linearity/nonlinearity with respect to the relative deformed position vector $(\boldsymbol{\xi}+\boldsymbol{\eta})$. The nonlinearity of the integral kernel is meaningful, not only for modeling the physical behavior of those materials exhibiting a nonlinear stress–strain response or when really interesting phenomena (like solitons [81, 82]) appear, but also because it may be involved in predicting the onset of fractures in a material body. Let us consider the pairwise force equation (3.14), reported below for convenience, as representative of linear models

$$\mathbf{f}(\boldsymbol{\xi},\boldsymbol{\eta})=c(\boldsymbol{\xi},\delta)\frac{|\boldsymbol{\xi}+\boldsymbol{\eta}|-|\boldsymbol{\xi}|}{|\boldsymbol{\xi}|}\mu(s,t)\boldsymbol{n}, \tag{4.10}$$

where

$$\mu(s,t)=\begin{cases}1 & \text{if } s(t',\boldsymbol{\xi})<s_0,\\ 0 & \text{otherwise,}\end{cases}\qquad \text{for all } 0\le t'\le t, \tag{4.11}$$

we will refer to it as *linear kernel*; it is worth noting that the micromodulus function $c(\boldsymbol{\xi},\delta)$ is not a source of bond stretch nonlinearity because, once a bond $(\mathbf{x},\mathbf{x}')\equiv\bar{\boldsymbol{\xi}}$ is fixed, $c(\bar{\boldsymbol{\xi}},\delta)$ reduces to a constant. Let us consider, instead, as representative of nonlinear models, the pairwise force equation (3.22), reported below for convenience:

$$\mathbf{f}(\boldsymbol{\xi},\boldsymbol{\eta})=\kappa p\frac{|\boldsymbol{\eta}+\boldsymbol{\xi}|^{p-2}}{|\boldsymbol{\xi}|^{N+\alpha p}}(\boldsymbol{\eta}+\boldsymbol{\xi})+\psi(\boldsymbol{\xi},\boldsymbol{\eta}). \tag{4.12}$$

We will refer to it as the *nonlinear kernel*. Regarding the linear kernel, it is notable that the only role of the function $\mu(s,t)$ is modeling crack formation and development in the material, and that the threshold value s_0 is only determined by measurable quantity [49]. If we consider the equivalent formulation of $\mu(s,t)$ proposed in [83]

$$\mu(s)=\Theta_\epsilon\left(\int_0^t\max\{0,s(\boldsymbol{\xi},\tau)-s_0\}\,\mathrm{d}\tau\right)\quad\text{for }\epsilon\to 0, \tag{4.13}$$

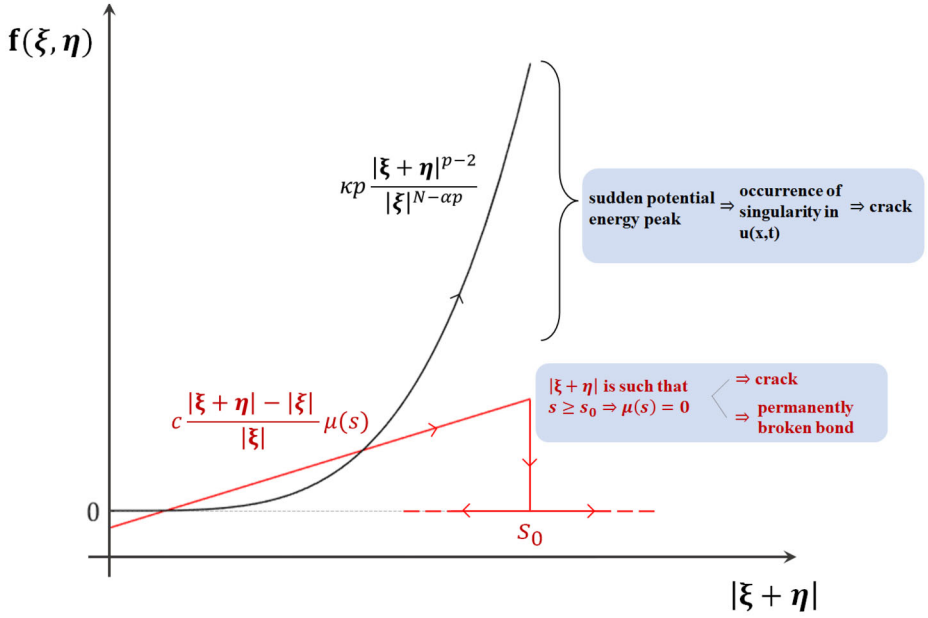

Figure 5 Generation of fractures and cracks with linear and nonlinear peridynamics kernels. *In red*, a typical linear peridynamics kernel $c(\boldsymbol{\xi},\delta)\frac{|\boldsymbol{\xi}+\boldsymbol{\eta}|-|\boldsymbol{\xi}|}{|\boldsymbol{\xi}|}\mu(s)\boldsymbol{n}$ is represented. After a bond is broken, the pairwise force remains indefinitely equal to the zero function. *In black*, a nonlinear peridynamics kernel $\kappa p\frac{|\boldsymbol{\eta}+\boldsymbol{\xi}|^{p-2}}{|\boldsymbol{\xi}|^{N+\alpha p}}(\boldsymbol{\eta}+\boldsymbol{\xi})$ is represented. Nonlinearity allows the formation of abrupt force and so potential energy peaks such that there is the occurrence of singularity in the displacement function

where

$$\Theta_\varepsilon(r) = \begin{cases} 1, & r \leq 0, \\ 1-\frac{r}{\varepsilon}, & 0 < r < \varepsilon, \\ 0, & r \geq \varepsilon, \end{cases} \tag{4.14}$$

then the mathematical well-posedness of the peridynamic equation related to the linear integral kernel with bond-braking function $\mu(s,t)$ can be proven (see [83] for a rigorous proof; for a different reformulation of the bond-braking function $\mu(s,t)$, where no time integration is involved and for which mathematical well-posedness of the peridynamic equation is also proved, see [84]). Notwithstanding its mathematical well-posedness, we can notice, looking at the linear pairwise force plot (see red line in Fig. 5), how this kind of model looks a bit artificial; in fact, a physical phenomenon described by a linear model is such that its behavior is indefinitely preserved, so that, within this setting, the onset of abrupt events (like cracks are) is unreasonable, except with a "forced from the outside" intervention. Considering, instead, the nonlinear kernel, we can see how this kind of pairwise force structure allows inherently the possibility of modeling sudden force intensity (and concurrently potential energy) escalations with respect to relatively low displacements. Potential energy peaks may be naturally identified with abrupt events, like cracks, which are phenomena that require great energy localization into the bound to take place (see black line in Fig. 5). Within the context of nonlinear kernels, the aforementioned *nonlinear crack* approach is capable of predicting cracks formation independently from external parameters, like s_0, and regardless of the degree of regularity of the initial condition,

but, on the other hand, it is not able to propagate cracks unless a *bond-breaking* function, as $\mu(s,t)$, is introduced.

5 Peridynamics in fluids: future perspectives

Now the perspective of rigorously extending the peridynamics formalism to fluids is given. The main motivation for such an extension is to develop a model for fluids that allow us to model nonlocal phenomena typically seen in complex fluids (like blood, polymeric flow, etc.), and at the same time to take the advantage of the mathematical soundness of PD theory with respect to arising discontinuities.

As it is well known, fluids and solids (i.e., elastic materials) exhibit very different physical behavior. Let us consider a simple clarifying example. If an elastic (solid) material is subjected to a pure shear deformation (e.g., the material is placed between two plates forced to move in opposite directions); we would expect, and it is what physically happens, that an equilibrium configuration will be reached in a certain amount of time, in the sense that the solid assumes a well definite shape so as to balance plate exerted forces. Now, if we would repeat the experiment for a fluid, then as time goes on, it keeps sliding with the plates, and no equilibrium shape is reached. On the other hand, looking at the fluid velocity, we can observe that each point assumes a well-defined average velocity profile, so that an equilibrium configuration is reached in the velocity field. We can conclude that in solids the "preferred" kinematic quantity is the displacement vector $\mathbf{u}$, whereas in fluid it is the infinitesimal variation of displacement with time, i.e., the velocity $\mathbf{u}_t$ assumes a key role. Such a fundamental distinction reflects, in the classical continuum mechanics framework, the structure of the governing equations for fluids and solids, respectively.

The main three ingredients in mechanical governing equations are kinematics relations, physically conserved quantities, and constitutive relations. For simplicity, in the following discussion, we neglect thermodynamic considerations, postponing a more comprehensive treatise for future investigations. Kinematics of elastic materials is essentially described by the deformation gradient:

$$\mathbf{F} := \nabla_{\mathbf{x}} \boldsymbol{\chi}, \tag{5.1}$$

recalling that $\chi(\mathbf{x},t) := \mathbf{x} + \mathbf{u}(\mathbf{x},t)$. For the balance equations, we adopt a referential structure, so that the mass, linear momentum, and angular momentum conservation read

$$\begin{aligned} &\rho = \rho_R / J, \\ &\rho_R \ddot{\chi} = \nabla_{\mathbf{x}} \cdot \mathbf{T}_R + \mathbf{b}_{0R}, \\ &\mathbf{T}_R \mathbf{F}^\top = \mathbf{F} \mathbf{T}_R^\top, \end{aligned} \tag{5.2}$$

where $J := \det \mathbf{F}$, and the subscript R denotes that a given quantity is considered in the reference configuration. Indeed, ρ_R is the density at point $\mathbf{x}$ in reference configuration, and T_R is the first Piola stress tensor. We assume the following constitutive relation:

$$\mathbf{T}_R = T_R(\mathbf{F}), \tag{5.3}$$

where T_R is a function directly linking the stress at a point of the body to its deformation gradient. Therefore, considering equations (5.1), (5.2), and (5.3) given below, fully describing the evolution of an elastic body, the fundamental role of $\mathbf{F}$ can be highlighted. From

that it appears clearly that $\mathbf{u}(x,t)$, i.e., the displacement of the material point $\mathbf{x}$ from its reference configuration, assumes a preferred status in elastic bodies due to its close relation with $\mathbf{F}$, namely $\mathbf{F} := \nabla_{\mathbf{x}}\chi = \mathbf{I} + \nabla_{\mathbf{x}}\mathbf{u}$.

Now let us consider kinematics, balance equations, and constitutive relation for incompressible fluids. Due to the absence of a physical meaningful reference configuration, kinematic relations are expressed only as a function of the geometrical space variables $\mathbf{z} \in \mathbb{R}^n$ (we use the symbol $\mathbf{z}$ instead of the classical x to sharply differentiate the geometrical space variable from the reference space variable $\mathbf{x}$). Now, identifying $\chi_t(\mathbf{x},t) = \chi((\chi^{-1}(\mathbf{z},t),t)$ with $\mathbf{v}(\mathbf{z},t)$, we express the motion of a given particle of a fluid continuum as follows:

$$\frac{D\mathbf{v}(\mathbf{z},t)}{Dt} = \mathbf{v}_t(\mathbf{z},t) + \big[\nabla_{\mathbf{z}}\mathbf{v}(\mathbf{z},t)\big]\mathbf{v}(\mathbf{z},t), \tag{5.4}$$

where D/Dt denotes the material derivative of the field $\mathbf{v}(\mathbf{z},t)$, and $\nabla_{\mathbf{z}}$ is the gradient operator with respect to geometrical space variables. The balance equations are consequently expressed as [80]

$$\begin{aligned} &\nabla_{\mathbf{z}} \cdot \mathbf{v} = 0, \\ &\rho\mathbf{v}_t = \nabla_{\mathbf{z}} \cdot (\mathbf{T} - \rho\mathbf{v} \otimes \mathbf{v}) + \mathbf{b}_0, \\ &\mathbf{T} = \mathbf{T}^{\top}, \end{aligned} \tag{5.5}$$

where $\mathbf{T}$ is the Cauchy stress tensor. For fluids that are in general non-Newtonian, we assume the following constitutive relation:

$$\mathbf{T} = T(\mathbf{D}), \tag{5.6}$$

where T is a function that links the stress at a fluid point to the stretching tensor

$$\mathbf{D} := \frac{1}{2}\big(\nabla_{\mathbf{z}}\mathbf{v} + \nabla_{\mathbf{z}}\mathbf{v}^{\top}\big), \tag{5.7}$$

which represents the stretching and angle changing rate of material fibers. A so-called Eulerian description of fluids has been presented. By looking at the equations that govern fluid motion we can notice the relevance of the velocity $\mathbf{v}$. Being $\chi_t(\mathbf{x},t) = \mathbf{u}_t(\mathbf{x},t)$ and $\chi_t(\mathbf{x},t) \equiv \mathbf{v}(\mathbf{z},t)$, the key role of $\mathbf{u}_t$ in fluid phenomenology is recovered. Thus, in the extension of the peridynamics formalism toward fluids, we expect that the velocity must possess a key role in the governing equation.

A first attempt to extend PD theory to fluids could be modeling the divergence of internal forces with a nonlocal term of integral type, $\int_{B_\delta} \mathbf{f}\, dV$, similarly to what has been done for elastic materials PD theory. However, unlike what happens for the Lagrangian form of linear momentum balance equation $(5.2)_2$, where all spatial derivatives (i.e., $\nabla_{\mathbf{x}}\cdot$) are replaced by the integral force term, this step would not work for the Eulerian form of linear momentum balance $(5.5)_2$, where $(\nabla_{\mathbf{z}}\cdot)$ does not appear only in the internal force term but also is inherent in fluid kinematics. Hence it is not surprising that the fluid peridynamics state-based models proposed in [12, 19] are based on a Lagrangian description of fluid and that a truly Eulerian peridynamics formulation has not been proposed yet.

An interesting feature brings together the proposed fluid PD models: if in elastic material the peridynamics horizon $B_\delta(\mathbf{x})$ is defined in the reference configuration and is composed

of the same material points during all body motion, in fluid, PD horizon maintains its spherical shape at every time t, so that different points at different time instants may belong to the horizon. The main explanation (see [19]) of such a divergent property of $B_\delta(\mathbf{x})$ relies on the fact that in fluids where deformations are very huge, it would be nonphysical to let points $\mathbf{x}$ and $\mathbf{x}'$ such that $|\mathbf{x}-\mathbf{x}'| \leq \delta$ in Ω_0 to keep interaction even if at a certain time, say $t = \tau$, $\mathbf{y} = \chi(\mathbf{x})$ and $\mathbf{y}' = \chi(\mathbf{x}')$ in Ω_τ are such that $|\mathbf{y}-\mathbf{y}'| \gg \delta$. Such differences between fluid and solid in the definition of the PD horizon may be regarded in a different light, by the introduction of *fading memory* concept. Fading memory in materials was firstly introduced by Boltzmann [85] and Volterra [86] and formalized by Colemann and Noll [87] in the framework of continuum mechanics; the main assumption is that the stress in a material body depends upon the history of its past configurations up to a certain remembered time. Specifically, the concept of fading memory is based on the following argument: the stress-free configuration for the elastic material cannot be recovered instantaneously as soon as the interaction has acted. Indeed, liquid materials instantly "forget" their already acquired deformations since any state is an equilibrium state: this is why liquids are considered without memory. On the contrary, elastic materials do not forget the history of their deformations at all. So their memory does not fade. In this context the difference between elastic materials and fluids is related to their memory: an elastic material is such that it remembers its "original" configuration, i.e., possesses infinite memory, and thus tries to restore its initial shape at any time. On the opposite hand, a fluid is a material with zero memory, so that a reference or "original" configuration cannot be found [88].

In the following, we present a nonrigorous but interesting and stimulating perspective of the application of the concept of fading memory in the development of a peridynamics model for fluids. Consider a material body and let the parameter s, with the dimension of time, denote the memory of the material, so that the material can remember only up to time $t-s$. So if $s \to \infty$, then the material is perfectly elastic, whereas if $s \to 0$, then we obtain a fluid behavior. Extend the displacement function extended in the time variable to $\tilde{\mathbf{u}}(\mathbf{x},t) : \Omega_0 \in \mathbb{R}^n \times \mathbb{R} \to \mathbb{R}^n$ such that

$$\tilde{\mathbf{u}}(\mathbf{x},t) := \begin{cases} \mathbf{u}(\mathbf{x},t) & \text{for } t \geq 0, \\ \mathbf{0} & \text{for } t < 0, \end{cases} \tag{5.8}$$

and let us consider the consequent extension of $\chi(\mathbf{x},t)$ so that $\chi(\mathbf{x},t) := \mathbf{x} + \tilde{\mathbf{u}}(\mathbf{x},t)$. In standard PD theory the internal force acting at point $\mathbf{x}$ at time $t = \tau$ is of elastic nature and directly depends on the deformation of $B_\delta(\mathbf{x})$ at $t = \tau$. A straightforward extension of this peridynamics concept of internal force to materials with memory s is to consider the deformation of the peridynamics horizon with respect to its last remembered configuration

$$B_\delta(\mathbf{x},t-s) := \left\{\mathbf{z} \in \mathbb{R}^n : \left\| \chi(\mathbf{x},t-s) - \mathbf{z} \right\| < \delta\right\}. \tag{5.9}$$

Consequently, internal forces acting at $\mathbf{x}$ are related to the current deformation (at time t) of $B_\delta(\mathbf{x},t-s)$, which is thus taken as a reference configuration. It is worth noting that in this new framework the horizon assumes a more geometrical structure, in contrast with the classical definition, by which it is defined as a set of fixed material points. At the moment, boundaries are neglected, so that the horizon is never empty, i.e.,

$$\forall \mathbf{z} \in B_\delta(\mathbf{x},t)\ \exists \mathbf{x}' \in \Omega_0 \text{ such that } \mathbf{z} = \chi\left(\mathbf{x}',t\right).$$

Given the above considerations, it seems reasonable to extend the classical PD bond-based model to a generic material with memory s maintaining the same physical structure. Therefore the pairwise force $\mathbf{f}$ is regarded as a function of the relative position between $\mathbf{x}$ and a generic point in $B_\delta(\mathbf{x}, t-s)$ in the reference configuration (time $t-s$) and of their current relative displacement (time t) with respect to the reference configuration. As a consequence, the peridynamics balance of the linear momentum equation follows:

$$\begin{aligned}\rho\chi_{tt}(\mathbf{x},t) = \int_{\Omega_0\cap B_\delta(\mathbf{x},t-s)} \mathbf{f}\Big(& \underbrace{\mathbf{z}-\chi(\mathbf{x},t-s)}_{\text{relative position between } \mathbf{x} \text{ and } \mathbf{z}}, \\ & \underbrace{\chi\big(\chi^{-1}(\mathbf{z},t-s),t\big)-\chi\big(\chi^{-1}(\mathbf{z},t-s),t-s\big)}_{\text{displacement of } \mathbf{z} \text{ from reference config.}} \\ & - \underbrace{\big[\chi(\mathbf{x},t)-\chi(\mathbf{x},t-s)\big]}_{\text{displacement of } \mathbf{x} \text{ from reference config.}} \Big)\, dV_{\mathbf{z}}.\end{aligned} \tag{5.10}$$

If a solid material is considered, i.e., $s\to\infty$, assuming necessary smoothness with respect to the time variable for all involved functions, we get

$$\begin{aligned}&\lim_{s\to\infty}\int_{\Omega_0\cap B_\delta(\mathbf{x},t-s)} \mathbf{f}\big(\mathbf{z}-\chi(\mathbf{x},t-s),\chi\big(\chi^{-1}(\mathbf{z},t-s),t\big) \\ &\qquad -\chi\big(\chi^{-1}(\mathbf{z},t-s),t-s\big)-\big[\chi(\mathbf{x},t)-\chi(\mathbf{x},t-s)\big]\big)\,dV_{\mathbf{z}} \\ &= \int_{\Omega_0\cap B_\delta(\mathbf{x})} \mathbf{f}\big(\mathbf{x}'+\mathbf{x},\chi\big(\mathbf{x}',t\big)-\mathbf{x}'-\chi(\mathbf{x},t)+\mathbf{x}]\big)\,dV_{\mathbf{x}'} \\ &= \int_{\Omega_0\cap B_\delta(\mathbf{x})} \mathbf{f}\big(\mathbf{x}'+\mathbf{x},\mathbf{x}'+\tilde{\mathbf{u}}\big(\mathbf{x}',t\big)-\mathbf{x}'-\mathbf{x}-\tilde{\mathbf{u}}(\mathbf{x},t)+\mathbf{x}\big)\,dV_{\mathbf{x}'} \\ &= \int_{\Omega_0\cap B_\delta(\mathbf{x})} \mathbf{f}(\boldsymbol{\xi},\boldsymbol{\eta})\,dV_{\mathbf{x}'},\end{aligned} \tag{5.11}$$

remembering that, as $(t-s)\to-\infty$, $\tilde{\mathbf{u}}(\cdot,t-s)\to\mathbf{0}$, and thus $B_\delta(\mathbf{x},t-s)\ni\mathbf{z}\equiv\mathbf{x}'\in B_\delta(\mathbf{x})$. The standard bond-based PD equation has been recovered. If the limit of (5.10) as $s\to 0$ is taken, then we expect to obtain, almost formally, a peridynamic equation for incompressible fluids. Lets first consider a first-order Taylor expansion in the time variable, so that

$$\begin{aligned}\rho\chi_{tt}(\mathbf{x},t) = \int_{\Omega_0\cap B_\delta(\mathbf{x},t-s)} & \mathbf{f}\big(\mathbf{z}-\chi(\mathbf{x},t-s), \\ & \big[\chi_t\big(\chi^{-1}(\mathbf{z},t-s),t\big)-\chi_t(\mathbf{x},t)\big]s+o(s)\big)\,dV_{\mathbf{z}}.\end{aligned} \tag{5.12}$$

Thus, under suitable regularity assumptions with respect to the time variable, letting $s\to 0$, it follows that

$$\rho\chi_{tt}(\mathbf{x},t) = \int_{\Omega_0\cap B_\delta(\mathbf{x},t)} \mathbf{f}\big(\mathbf{z}-\chi(\mathbf{x},t),\big[\mathbf{v}(\mathbf{z},t)-\chi_t(\mathbf{x},t)\big]\delta s\big)\,dV_{\mathbf{z}}, \tag{5.13}$$

where δs is an infinitesimal time interval ($\delta s\ll 1$) we can get rid of by a slightly modification of (5.10), and where the correspondence $\mathbf{v}(\mathbf{z},t)\equiv\chi_t(\chi^{-1}(\mathbf{z},t))$ has been employed. It

is interesting to note that, similarly to classical constitutive relations for fluid (5.6), the actual velocity difference between **x** and others surrounding point in its horizon is involved in the peridynamic kernel and thus determines the constitutive behavior of the fluid. By employing the concept of fading memory the key role of velocity in fluid material has been recovered, almost formally. On the other hand, a redefinition of the peridynamic horizon from a set of material points to a purely geometrical one brings extra complications. Indeed, in (5.13) the geometric and material velocity is mingled so that the model is neither Lagrangian nor Eulerian. We must stress that the present formulation is only suitable for describing isotropic and fully periodic flows. Future studies will include the description of the boundaries and the role of the choice of the specific strategy for enforcing no-slip conditions in the peridynamic realm.

6 Conclusions

A wide-breath review of bond-based peridynamic theory has been presented. Features, applications, and numerical methods involved in bond-based and state-based PD have been briefly described; then the paper focuses on the bond-based PD formulation of solid mechanics. Basic physical principles that shape peridynamics integral kernels are described. Then a review of the most common kernels employed in the literature is presented. By a comparison of the various kernel, it has been shown that, apart from the micromodulus function, which can be quite general, all the models share a rational function structure. It has been shown that PD kernels are derived from exact kinematics, i.e., at all scales, no approximations of displacement of points are assumed. Implications of material impenetrability constrain on the kernel structures have been analyzed. A necessary but insufficient condition for material impenetrability has been related to the presence of a denominator of type $|\boldsymbol{\xi}|^{\beta}$ with some real number β, which goes to zero in the analytical integration process. On the other hand, in a numerical integration process, this condition has no meaning (the denominator is mesh dependent and thus never reaches a zero value), so that future research in numerical peridynamics may be directed toward the resolution of such discrepancy. The potential role of employing a nonlinear PD kernel in predicting the onset of fractures has been explored. Cracks formation modeling capacity of widely employed linear kernels supplemented with a bond-breaking function is qualitatively compared with a nonlinear kernel. As a result, it appears that the presence of nonlinearity in the relative displacement can reproduce inherently the high potential energy peaks that indicate the formation process of cracks. Further numerical studies on nonlinear kernels will be performed to test their accuracy in predicting crack formation. Finally, some research perspectives on the extension of bond-based PD toward fluids have been offered. The prominent behavior difference between solids and fluids has been related to the preferred status of deformation in solids and deformation rate in fluids. Then the implications of extending the peridynamics formalism toward fluids have been analyzed via the materials memory concept. In this unifying framework the main ideas of peridynamics have been extended formally toward fluids. The key role of the deformation rate has been recovered, but, on the other end, the necessary redefinition of the PD horizon from a material set to a geometric one leads to a PD governing equation in which geometric and material quantities are blended. Future research will be directed toward a more clear understanding of the implications of PD nonlocality on the relation between Lagrangian (material) and Eulerian (geometric) descriptions of materials.

Acknowledgements
AC acknowledges the project "Research for Innovation" (REFIN) – POR Puglia FESR FSE 2014-2020 - Asse X - Azione 10.4 (Grant No. CUP - D94120001410008). AC and TP are members of Gruppo Nazionale per il Calcolo Scientifico (GNCS) of Istituto Nazionale di Alta Matematica (INdAM). GF acknowledges the support by Fundacao para a Ciencia e a Tecnologia (FCT) under the program "Stimulus" with grant no. CEECIND/04399/2017/CP1387/CT0026 and through the research project with ref. number PTDC/FIS-AST/0054/2021. GF is also a member of the Gruppo Nazionale per la Fisica Matematica (GNFM) of the Istituto Nazionale di Alta Matematica (INdAM).

Funding
This work was partially supported by the project "Research for Innovation" (REFIN) – POR Puglia FESR FSE 2014-2020 - Asse X - Azione 10.4 (Grant No. CUP - D94120001410008) and Fundacao para a Ciencia e a Tecnologia (FCT) under the program "Stimulus" with grant no. CEECIND/04399/2017/CP1387/CT0026 and through the research project with ref. number PTDC/FIS-AST/0054/2021.

Availability of data and materials
The datasets used and/or analyzed during the current study are available from the corresponding author on reasonable request.

Declarations

Ethics approval and consent to participate
The authors approve the ethics of the journal and give the consent to participate.

Consent for publication
The authors consent for the publication.

Competing interests
The authors declare no competing interests.

Author contribution
The authors declare that they gave their individual contributions in every section of the manuscript. All authors read and approved the final manuscript.

Author details
[1]Dipartimento di Ingegneria Elettrica e dell'Informazione, Politecnico di Bari, Via Re David 200, 70125 Bari, Italy. [2]Instituto de Astrofisíca e Ciências do Espaço, Faculdade de Ciências, Universidade de Lisboa, Edificio C8, Campo Grande, P-1749-016, Lisbon, Portugal.

Publisher's Note

Received: 5 August 2022 Accepted: 12 October 2022 Published online: 23 October 2022

References

1. Silling, S.A.: Reformulation of elasticity theory for discontinuities and long-range forces. J. Mech. Phys. Solids **48**(1), 175–209 (2000). https://doi.org/10.1016/S0022-5096(99)00029-0. ISSN 0022-5096
2. Javili, A., Morasata, R., Oterkus, E., Oterkus, S.: Peridynamics review. Math. Mech. Solids **24**(11), 3714–3739 (2019)
3. Coclite, G.M., Dipierro, S., Fanizza, G., Maddalena, F., Romano, M., Valdinoci, E.: Qualitative aspects in nonlocal dynamics. J. Peridyn. Nonlocal Model. (2021). https://doi.org/10.1007/s42102-021-00064-z
4. Seleson, P., Parks, M.L., Gunzburger, M., Lehoucq, R.B.: Peridynamics as an upscaling of molecular dynamics. Multiscale Model. Simul. **8**(1), 204–227 (2009)
5. Butt, S.N., Timothy, J.J., Meschke, G.: Wave dispersion and propagation in state-based peridynamics. Comput. Mech. **60**(5), 725–738 (2017)
6. Bažant, Z.P., Luo, W., Chau, V.T., Bessa, M.A.: Wave dispersion and basic concepts of peridynamics compared to classical nonlocal damage models. J. Appl. Mech. **83**(11), 111004 (2016)
7. Ha, Y.D., Bobaru, F.: Studies of dynamic crack propagation and crack branching with peridynamics. Int. J. Fract. **162**(1), 229–244 (2010)
8. Agwai, A., Guven, I., Madenci, E.: Predicting crack propagation with peridynamics: a comparative study. Int. J. Fract. **171**(1), 65–78 (2011)
9. Ni, T., Zaccariotto, M., Zhu, Q.-Z., Galvanetto, U.: Static solution of crack propagation problems in peridynamics. Comput. Methods Appl. Mech. Eng. **346**, 126–151 (2019)
10. Lipton, R.: Dynamic brittle fracture as a small horizon limit of peridynamics. J. Elast. **117**(1), 21–50 (2014)
11. Silling, S.A., Weckner, O., Askari, E., Bobaru, F.: Crack nucleation in a peridynamic solid. Int. J. Fract. **162**(1), 219–227 (2010)
12. Behzadinasab, M., Vogler, T.J., Peterson, A.M., Rahman, R., Foster, J.T.: Peridynamics modeling of a shock wave perturbation decay experiment in granular materials with intra-granular fracture. J. Dyn. Behav. Mater. **4**(4), 529–542 (2018)
13. Askari, E., Bobaru, F., Lehoucq, R.B., Parks, M.L., Silling, S.A., Weckner, O.: Peridynamics for multiscale materials modeling. J. Phys. Conf. Ser., **125**, 012078 (2008)

14. Madenci, E., Oterkus, E.: Peridynamic theory. In: Peridynamic Theory and Its Applications, Springer, Berlin, pp. 19–43 (2014)
15. Macek, R.W., Silling, S.A.: Peridynamics via finite element analysis. Finite Elem. Anal. Des. **43**(15), 1169–1178 (2007)
16. Sarego, G., Le, Q.V., Bobaru, F., Zaccariotto, M., Galvanetto, U.: Linearized state-based peridynamics for 2-d problems. Int. J. Numer. Methods Eng. **108**(10), 1174–1197 (2016)
17. Zaccariotto, M., Luongo, F., Galvanetto, U., et al.: Examples of applications of the peridynamic theory to the solution of static equilibrium problems. Aeronaut. J. **119**(1216), 677–700 (2015)
18. Silling, S.A., Epton, M., Weckner, O., Xu, J., Askari, E.: Peridynamic states and constitutive modeling. J. Elast. **88**(2), 151–184 (2007)
19. Silling, S.A., Parks, M.L., Kamm, J.R., Weckner, O., Rassaian, M.: Modeling shockwaves and impact phenomena with Eulerian peridynamics. Int. J. Impact Eng. **107**, 47–57 (2017)
20. Behzadinasab, M., Foster, J.T.: A semi-Lagrangian constitutive correspondence framework for peridynamics. J. Mech. Phys. Solids **137**, 103862 (2020)
21. Ni, T., Pesavento, F., Zaccariotto, M., Galvanetto, U., Zhu, Q.-Z., Schrefler, B.A.: Hybrid FEM and peridynamic simulation of hydraulic fracture propagation in saturated porous media. Comput. Methods Appl. Mech. Eng. **366**, 113101 (2020)
22. Zhou, X.-P., Wang, Y.-T., Shou, Y.-D.: Hydromechanical bond-based peridynamic model for pressurized and fluid-driven fracturing processes in fissured porous rocks. Int. J. Rock Mech. Min. Sci. **132**, 104383 (2020)
23. Song, X., Khalili, N.: A peridynamics model for strain localization analysis of geomaterials. Int. J. Numer. Anal. Methods Geomech. **43**(1), 77–96 (2019)
24. Panchadhara, R., Gordon, P.A., Parks, M.L.: Modeling propellant-based stimulation of a borehole with peridynamics. Int. J. Rock Mech. Min. Sci. **93**, 330–343 (2017)
25. Zhou, X.-P., Wang, Y.-T.: State-of-the-art review on the progressive failure characteristics of geomaterials in peridynamic theory. J. Eng. Mech. **147**(1), 03120001 (2021)
26. Lejeune, E., Linder, C.: Modeling tumor growth with peridynamics. Biomech. Model. Mechanobiol. **16**(4), 1141–1157 (2017)
27. Taylor, M., Gözen, I., Patel, S., Jesorka, A., Bertoldi, K.: Peridynamic modeling of ruptures in biomembranes. PLoS ONE **11**(11), e0165947 (2016)
28. Bobaru, F., Duangpanya, M.: The peridynamic formulation for transient heat conduction. Int. J. Heat Mass Transf. **53**(19–20), 4047–4059 (2010)
29. Bobaru, F., Duangpanya, M.: A peridynamic formulation for transient heat conduction in bodies with evolving discontinuities. J. Comput. Phys. **231**(7), 2764–2785 (2012)
30. Oterkus, S., Madenci, E., Agwai, A.: Peridynamic thermal diffusion. J. Comput. Phys. **265**, 71–96 (2014)
31. Foster, J.T.: Nonlocal and fractional order methods for near-wall turbulence, large-eddy simulation, and fluid-structure interaction. Technical report, University of Texas at Austin Austin United States (2019)
32. Zhao, J., Chen, Z., Mehrmashhadi, J., Bobaru, F.: Construction of a peridynamic model for transient advection-diffusion problems. Int. J. Heat Mass Transf. **126**, 1253–1266 (2018)
33. Buryachenko, V.A.: Generalized effective fields method in peridynamic micromechanics of random structure composites. Int. J. Solids Struct. **202**, 765–786 (2020)
34. Hu, Y.L., Madenci, E.: Peridynamics for fatigue life and residual strength prediction of composite laminates. Compos. Struct. **160**, 169–184 (2017)
35. Oterkus, E., Madenci, E.: Peridynamic analysis of fiber-reinforced composite materials. J. Mech. Mater. Struct. **7**(1), 45–84 (2012)
36. Zhao, J., Jafarzadeh, S., Rahmani, M., Chen, Z., Kim, Y.-R., Bobaru, F.: A peridynamic model for galvanic corrosion and fracture. Electrochim. Acta **391**, 138968 (2021)
37. Wildman, R., Gazonas, G.: A dynamic electro-thermo-mechanical model of dielectric breakdown in solids using peridynamics. J. Mech. Mater. Struct. **10**(5), 613–630 (2015)
38. Randles, P.W., Libersky, L.D.: Smoothed particle hydrodynamics: some recent improvements and applications. Comput. Methods Appl. Mech. Eng. **139**(1–4), 375–408 (1996)
39. Ren, X.-H., Yu, S.-Y., Wang, H.-J., Zhang, J.-X., Sun, Z.-H.: An improved form of SPH method and its numerical simulation study on the rock crack propagation containing fissures and holes. Arab. J. Sci. Eng. **46**(11), 11303–11317 (2021)
40. Moës, N., Dolbow, J., Belytschko, T.: A finite element method for crack growth without remeshing. Int. J. Numer. Methods Eng. **46**(1), 131–150 (1999)
41. Rocha, A.V.M., Akhavan-Safar, A., Carbas, R., Marques, E.A.S., Goyal, R., El-zein, M., Da Silva, L.F.M.: Numerical analysis of mixed-mode fatigue crack growth of adhesive joints using CZM. Theor. Appl. Fract. Mech. **106**, 102493 (2020)
42. Shojaei, A., Hermann, A., Cyron, C.J., Seleson, P., Silling, S.A.: A hybrid meshfree discretization to improve the numerical performance of peridynamic models. Comput. Methods Appl. Mech. Eng. **391**, 114544 (2022)
43. Lopez, L., Pellegrino, S.F.: A space-time discretization of a nonlinear peridynamic model on a 2D lamina. Comput. Math. Appl. **116**, 161–175 (2022)
44. Coclite, G.M., Fanizzi, A., Lopez, L., Maddalena, F., Pellegrino, S.F.: Numerical methods for the nonlocal wave equation of the peridynamics. Appl. Numer. Math. **155**, 119–139 (2020). https://doi.org/10.1016/j.apnum.2018.11.007. ISSN 0168-9274
45. Jafarzadeh, S., Larios, A., Bobaru, F.: Efficient solutions for nonlocal diffusion problems via boundary-adapted spectral methods. J. Peridyn. Nonlocal Model. **2**(1), 85–110 (2020)
46. Lopez, L., Pellegrino, S.F.: A spectral method with volume penalization for a nonlinear peridynamic model. Int. J. Numer. Methods Eng. **122**(3), 707–725 (2021). https://doi.org/10.1002/nme.6555
47. Lopez, L., Pellegrino, S.F.: A nonperiodic Chebyshev spectral method avoiding penalization techniques for a class of nonlinear peridynamic models. Int. J. Numer. Methods Eng. **123**(20), 4859–4876 (2022)
48. Liang, X., Wang, L., Xu, J., Wang, J.: The boundary element method of peridynamics. Int. J. Numer. Methods Eng. **122**(20), 5558–5593 (2021)
49. Silling, S.A., Askari, E.: A meshfree method based on the peridynamic model of solid mechanics. Comput. Struct. **83**(17–18), 1526–1535 (2005)
50. Emmrich, E., Weckner, O.: Analysis and numerical approximation of an integro-differential equation modeling non-local effects in linear elasticity. Math. Mech. Solids **12**(4), 363–384 (2007)

51. Seleson, P., Littlewood, D.J.: Convergence studies in meshfree peridynamic simulations. Comput. Math. Appl. **71**(11), 2432–2448 (2016)
52. Bessa, M.A., Foster, J.T., Belytschko, T., Liu, W.K.: A meshfree unification: reproducing kernel peridynamics. Comput. Mech. **53**(6), 1251–1264 (2014)
53. Bobaru, F., Yang, M., Alves, L.F., Silling, S.A., Askari, E., Xu, J.: Convergence, adaptive refinement, and scaling in 1D peridynamics. Int. J. Numer. Methods Eng. **77**(6), 852–877 (2009)
54. Le, Q.V., Bobaru, F.: Surface corrections for peridynamic models in elasticity and fracture. Comput. Mech. **61**(4), 499–518 (2018)
55. Bobaru, F., Ha, Y.D.: Adaptive refinement and multiscale modeling in 2D peridynamics. Int. J. Multiscale Comput. Eng. **9**(6), 635–659 (2011)
56. Dipasquale, D., Zaccariotto, M., Galvanetto, U.: Crack propagation with adaptive grid refinement in 2D peridynamics. Int. J. Fract. **190**(1), 1–22 (2014)
57. Ren, H., Zhuang, X., Cai, Y., Rabczuk, T.: Dual-horizon peridynamics. Int. J. Numer. Methods Eng. **108**(12), 1451–1476 (2016)
58. Gu, X., Zhang, Q., Xia, X.: Voronoi-based peridynamics and cracking analysis with adaptive refinement. Int. J. Numer. Methods Eng. **112**(13), 2087–2109 (2017)
59. Shojaei, A., Mossaiby, F., Zaccariotto, M., Galvanetto, U.: An adaptive multi-grid peridynamic method for dynamic fracture analysis. Int. J. Mech. Sci. **144**, 600–617 (2018)
60. Henke, S.F., Shanbhag, S.: Mesh sensitivity in peridynamic simulations. Comput. Phys. Commun. **185**(1), 181–193 (2014)
61. Kilic, B., Madenci, E.: Coupling of peridynamic theory and the finite element method. J. Mech. Mater. Struct. **5**(5), 707–733 (2010)
62. Chen, X., Gunzburger, M.: Continuous and discontinuous finite element methods for a peridynamics model of mechanics. Comput. Methods Appl. Mech. Eng. **200**(9–12), 1237–1250 (2011)
63. Liu, Z., Cheng, A., Wang, H.: An hp-Galerkin method with fast solution for linear peridynamic models in one dimension. Comput. Math. Appl. **73**(7), 1546–1565 (2017)
64. Wang, H., Tian, H.: A fast Galerkin method with efficient matrix assembly and storage for a peridynamic model. J. Comput. Phys. **231**(23), 7730–7738 (2012)
65. Huang, X., Bie, Z., Wang, L., Jin, Y., Liu, X., Su, G., He, X.: Finite element method of bond-based peridynamics and its ABAQUS implementation. Eng. Fract. Mech. **206**, 408–426 (2019)
66. Zaccariotto, M., Tomasi, D., Galvanetto, U.: An enhanced coupling of PD grids to FE meshes. Mech. Res. Commun. **84**, 125–135 (2017)
67. Zaccariotto, M., Mudric, T., Tomasi, D., Shojaei, A., Galvanetto, U.: Coupling of FEM meshes with peridynamic grids. Comput. Methods Appl. Mech. Eng. **330**, 471–497 (2018)
68. Galvanetto, U., Mudric, T., Shojaei, A., Zaccariotto, M.: An effective way to couple FEM meshes and peridynamics grids for the solution of static equilibrium problems. Mech. Res. Commun. **76**, 41–47 (2016)
69. Zhang, Y., Madenci, E.: A coupled peridynamic and finite element approach in ANSYS framework for fatigue life prediction based on the kinetic theory of fracture. J. Peridyn. Nonlocal Model. **4**(1), 51–87 (2022)
70. Zheng, G., Shen, G., Xia, Y., Hu, P.: A bond-based peridynamic model considering effects of particle rotation and shear influence coefficient. Int. J. Numer. Methods Eng. **121**(1), 93–109 (2020)
71. Han, D., Zhang, Y., Wang, Q., Lu, W., Jia, B.: The review of the bond-based peridynamics modeling. J. Micromech. Mol. Phys. **4**(1), 1830001 (2019)
72. Silling, S.A., Bobaru, F.: Peridynamic modeling of membranes and fibers. Int. J. Non-Linear Mech. **40**(2–3), 395–409 (2005)
73. Chen, Z., Ju, J.W., Su, G., Huang, X., Li, S., Zhai, L.: Influence of micro-modulus functions on peridynamics simulation of crack propagation and branching in brittle materials. Eng. Fract. Mech. **216**, 106498 (2019)
74. Kilic, B.: Peridynamic theory for progressive failure prediction in homogeneous and heterogeneous materials. The University of Arizona (2008)
75. Chen, Z., Bakenhus, D., Bobaru, F.: A constructive peridynamic kernel for elasticity. Comput. Methods Appl. Mech. Eng. **311**, 356–373 (2016)
76. Madenci, E., Barut, A., Futch, M.: Peridynamic differential operator and its applications. Comput. Methods Appl. Mech. Eng. **304**, 408–451 (2016)
77. Huang, D., Lu, G., Wang, C., Qiao, P.: An extended peridynamic approach for deformation and fracture analysis. Eng. Fract. Mech. **141**, 196–211 (2015)
78. Coclite, G.M., Dipierro, S., Maddalena, F., Valdinoci, E.: Wellposedness of a nonlinear peridynamic model. Nonlinearity **32**(1), 1–21 (2018). https://doi.org/10.1088/1361-6544/aae71b. ISSN 1361-6544
79. Coclite, G.M., Dipierro, S., Fanizza, G., Maddalena, F., Valdinoci, E.: Dispersive effects in a peridynamic model. arXiv preprint, arXiv:2105.01558 (2021)
80. Gurtin, M.E., Fried, E., Anand, L.: The Mechanics and Thermodynamics of Continua. Cambridge University Press, Cambridge (2010)
81. Silling, S.A.: Solitary waves in a peridynamic elastic solid. J. Mech. Phys. Solids **96**, 121–132 (2016)
82. Pego, R.L., Van, T.-S.: Existence of solitary waves in one dimensional peridynamics. J. Elast. **136**(2), 207–236 (2019)
83. Emmrich, E., Puhst, D.: A short note on modeling damage in peridynamics. J. Elast. **123**(2), 245–252 (2016)
84. Du, Q., Tao, Y., Tian, X.: A peridynamic model of fracture mechanics with bond-breaking. J. Elast. **132**(2), 197–218 (2018). https://doi.org/10.1007/s10659-017-9661-2. ISSN 0374-3535
85. Boltzmann, L.: Zur Theorie der elastischen Nachwirkung. Ann. Phys. **241**(11), 430–432 (1878)
86. Volterra, V.: Sur les équations intégro-différentielles et leurs applications. Acta Math. **35**, 295 (1912)
87. Coleman, B.D., Noll, W.: Foundations of linear viscoelasticity. Rev. Mod. Phys. **33**(2), 239 (1961)
88. Astarita, G., Marrucci, G., Joseph, D.D.: Principles of non-Newtonian fluid mechanics. J. Appl. Mech. **42**(3), 750 (1975)